Modeling Ignition of A Heptane Isomer: Improved Thermodynamics, Reaction Pathways, Kinetic, and Rate Rule Optimizations for 2-Methylhexane

Samah Y. Mohamed[1], Liming Cai[2], Fethi Khaled[1], Colin Banyon[3], Zhandong Wang[1], Mariam J. Al Rashidi[1], Heinz Pitsch[2], Henry J. Curran[3], Aamir Farooq[1], S. Mani Sarathy[1]*

1 King Abdullah University of Science and Technology, Clean Combustion Research Center, Thuwal, 23955-6900, Saudi Arabia

2 Institute for Combustion Technology, RWTH Aachen University, 52062 Aachen, Germany

3 Combustion Chemistry Centre, Ryan Institute, School of Chemistry, National University of Ireland Galway, Ireland

ABSTRACT

Accurate chemical kinetic combustion models of lightly branched alkanes (e.g., 2-methylalkanes) are important to investigate the combustion behavior of real fuels. Improving the fidelity of existing kinetic models is a necessity, as new experiments and advanced theories show inaccuracies in certain portions of the models. This study focuses on updating thermodynamic data and the kinetic reaction mechanism for a gasoline surrogate component, 2-methylhexane,

based on recently published thermodynamic group values and rate rules derived from quantum calculations and experiments. Alternative pathways for the isomerization of peroxy-alkylhydroperoxide (OOQOOH) radicals are also investigated. The effects of these updates are compared against new high-pressure shock tube and rapid compression machine ignition delay measurements. It is shown that rate constant modifications are required to improve agreement between kinetic modeling simulations and experimental data. We further demonstrate the ability to optimize the kinetic model using both manual and automated techniques for rate parameter tunings to improve agreement with the measured ignition delay time data. Finally, additional low temperature chain branching reaction pathways are shown to improve the model's performance. The present approach to model development provides better performance across extended operating conditions while also strengthening the fundamental basis of the model.

1. Introduction

Accurate kinetic models of fuel oxidation at high and low temperatures offer better predictions of combustion properties, hence, enabling improvements in engine combustion efficiency with lower emissions. However, developing these models is challenging for complex fuels such as gasoline. In order to make kinetic model development more tractable, surrogate fuels are formulated such that they replicate the combustion properties of real fuels, including H/C ratio, distillation curve, and ignition quality, among others.

Chemical kinetic models consist of kinetic, thermodynamic, and transport data. One way of developing these mechanisms is via automated mechanism generators that make use of rate-based algorithms[1]. Alternatively, these models can be developed manually based on rate rule and group additivity methods for kinetic and thermodynamic data, respectively. Ideally, the rate coefficients of elementary reactions are taken from experimental measurements or theoretical

calculations. However, such data is often unavailable in the literature, which necessitates the use of estimation and analogy, and ultimately increases the level of uncertainty in the model. Thermodynamic data, on the other hand, is mainly estimated based on Group Additivity (GA) methods[2-4]. The accuracy of the thermodynamic data depends on that of the group values used.

Over the past few years, much effort has focused on the investigation of combustion reaction kinetics and thermodynamics, which has resulted in more accurate rate coefficients and group values, as well as new reaction pathways. Kinetic models available in the literature have to be updated based on newly obtained data in order to improve their predictive capabilities. Moreover, the updated models have to be compared against experimental data available in the literature. The kinetic models for C_5, C_6 and C_7 alkanes have been recently updated[5-7]. Silke et al.[7] updated the *n*-heptane model originally developed by Curran et al.[8]. In addition to updating the rate coefficients of existing reactions, they added new pathways for RO_2 + OH, RO_2 + HO_2, cyclic ether formation, and OOQOOH alternative isomerization reactions. Bugler et al.[5] revisited the chemical kinetic models of the pentane isomers originally developed by Healy et al.[9]. In their work, they investigated the effect of implementing thermodynamic and reaction rate updates[10-15], as well as the addition of alternative OOQOOH isomerization pathways, on the combustion properties of pentane isomers. Finally, *n*-hexane sub-mechanism in Curran et al.'s[8] heptane model was updated by Zhang et al.[6]. Reaction rate coefficients were updated and missing pathways were included. The updated mechanism was manually tuned (i.e., modified), within uncertainty limits, to provide better agreement with experimental data.

In this study, a kinetic model for 2-methylhexane, a molecule which has been proposed as a surrogate component for iso-alkanes in the middle boiling range of gasoline fuels[16], is updated and re-evaluated. The high-temperature mechanism for 2-methylhexane oxidation was initially

proposed by Westbrook et al.[17] as part of an experimental and modeling study on the heptane isomers. Later, Sarathy et al.[18] updated this mechanism and added low-temperature oxidation pathways based on Curran et al.'s models for *n*-heptane and iso-octane[8, 19]. In addition to updating the reaction rate parameters and base chemistry, Sarathy et al.[18] added concerted elimination pathways to the model. The updated mechanism was compared against rapid compression machine measurements performed by Silke et al.[20], and it was shown that the implemented updates improve agreement with the experimental data. Since the publication of Sarathy et al.'s[18] work, important advancements have been made in the field of combustion kinetics and thermodynamics. Therefore, the 2-methylhexane oxidation mechanism needs to be revisited yet again.

This work investigates the effects of updating the thermochemistry, reaction pathways, and rate rules on the simulated ignition kinetics of 2-methylhexane/air mixtures. The updated model is based on that of Sarathy et al.[18], and is compared against new shock tube and rapid compression machine ignition delay data. In order to ameliorate agreement between model and experiments, the rate coefficients of reactions with high sensitivity coefficients are modified. The modifications are effectuated via (i) manual tuning and (ii) automated optimization based on the methods proposed by Cai and Pitsch[21-22].

2. Experimental methods

The original 2-methylhexane model proposed by Sarathy et al.[18] was previously compared against rapid compression machine (RCM) ignition delay data from Silke et al.[20] at stoichiometric conditions and at end of compression pressures and temperatures of 13.5–15 bar and 640–960 K, respectively. The model updated herein is compared against the same experimental data. However, in order to further ensure the validity of this model, more

experiments are conducted over a wider range of conditions. RCM experiments were carried out at NUI Galway at pressures of 10, 15, 20, and 40 bar and equivalence ratios of 0.5 and 1.0. Moreover, experimental ignition delay data at high temperatures were obtained using the high-pressure shock tube at KAUST for pressures of 20 and 40 bar, and equivalence ratios of 0.5 and 1.0.

2.1 High Pressure Shock Tube measurements

Ignition delay times of 2-methylhexane/air mixtures were measured using the high-pressure shock tube (HPST) facility at KAUST. The shock tube is constructed from stainless steel with an inner diameter of 10 cm. The driven section is 6.6 m long and the driver section has a modular design to vary its length from 2.2 m to a maximum of 6.6 m. The mid-section of the tube houses two pre-scored aluminum diaphragms in a double-diaphragm arrangement (DDA) which allows better control of the post-reflected shock conditions compared to single diaphragm arrangement (SDA). The main difference between DDA and SDA is the diaphragm rupture timing. In SDA, the gas pressure in the driver section is increased until the diaphragm ruptures. The breaking pressure depends on many variables such as diaphragm thickness, scoring depth, aluminum grade and rate of pressure increase. This makes it hard to precisely control the bursting pressure (*p4*) and conditions (*p5* and T5) behind the reflected shock wave. In DDA, the mid-section is filled with bath gas at a pressure that is much lower than the breaking pressure of the diaphragm. Thereafter, the driver section is filled to the desired pressure *p4*. Breaking of the diaphragms is activated by suddenly venting the mid-section. This procedure allows precise control of post-shock temperature/pressure and experimental conditions can be easily reproduced[23].

The incident shock speed was measured using five PCB 113B26 piezoelectric pressure transducers (PZTs) placed in the last 3.6 m of the driven section. Shock attenuation rates varied

from 0.2 to 1.8 %/ms. Shock jump relations and known thermodynamic parameters were used to calculate the post-reflected shock conditions (*p5* and T5) with an uncertainty of < 1%. Sidewall pressure trace was measured using a Kistler 603B1 PZT located at 1.0 cm from the endwall. Also, OH* chemilimuniscence at 307 nm was monitored through sapphire windows at the endwall and sidewall (1.0 cm from the endwall) locations using modified Thorlabs PDA36A photo-detectors. A 3.39 μm He-Ne laser absorption diagnostic was set up at the sidewall location to measure fuel decay during the induction phase. The C–H stretching vibration in the fuel molecule causes absorption of 3.39 μm wavelength. This diagnostic can be used to measure only qualitative fuel decay profiles as other intermediate hydrocarbons also absorb laser light at this wavelength. A fast time-response photo-detector (VIGO Systems PVI-3TE-4) was used to collect the transmitted He-Ne signal. A schematic of the experimental setup is shown in Figure 1. A more detailed description of the experimental method could be found in[24].

2-Methylhexane was purchased from Sigma Aldrich (99% purity), whereas research-grade oxygen and nitrogen cylinders (99.999% purity) were purchased from Abdullah Hashim Gas Company. A molar ratio of 3.76:1.0 of N_2:O_2 was used to prepare fuel/air mixtures in a magnetically-stirred mixing tank. After vacuuming the mixing tank to pressures less than 1×10^{-4} mbar, 2-methylhexane was injected directly in the heated (75 ºC) mixing tank. The injection was made through a septa rubber valve that has high sealing properties. Mixing tank, manifold and shock tube driven section were electrically heated to 75 ºC to prevent condensation of 2-methylhexane. Driver gas tailoring (nitrogen in helium) and long length of driver section were used to extend the shock tube test times to 10 ms. A gradual pressure rise behind reflected shock wave (d*p5*/dt) was observed, which varied from 2–3%/ms.

Ignition delay time experiments spanned two equivalence ratios (0.5 and 1.0) and two pressures (20 and 40 bar). Reflected shock temperatures ranged 758-1280 K for the 40 bar experiments and 740–1290 K for the 20 bar data. Mixture compositions used for fuel-lean and stoichiometric ignition measurements are summarized in Table 1. Representative ignition delay time measurements are shown in Figure 2 and Figure 3. Time zero was defined as the time of mid-point of pressure jump from *p2* (pressure behind the incident shock wave) to *p5* (pressure behind the reflected shock wave). The onset of ignition was defined by the maximum slope in the sudden increase of pressure, OH* sidewall, OH* endwall or He-Ne laser signal. All four methods lead to very similar ignition delay times. Ignition delay data presented in this work are deduced from the pressure signal. A two-stage ignition phenomenon was clearly identified for 2-methylhexane at temperatures near 800 K for all conditions of pressure and equivalence ratio. The pressure jump due to first stage ignition was quite small at some conditions. For this reason, the He-Ne laser signal, proportional to fuel decay, was used to identify the first stage ignition delay time when possible (see Figure 3). The ignition delay times investigated in this work ranged from 64 μs to 10.5 ms. Ignition delay time uncertainty analysis of the experimental method showed that shock tube data reported in this work have an uncertainty of ±20%. Tabulated results of ignition delay times as a function of pressure, temperature, and equivalence ratio are presented as Supplementary data.

Table 1: Mixture composition for 2-methylhexane ignition delay shock tube experiments

Equivalence Ratio	2-methylhexane	Oxygen	Nitrogen
0.5	0.95%	20.81%	78.24%
1	1.88%	20.61%	77.51%

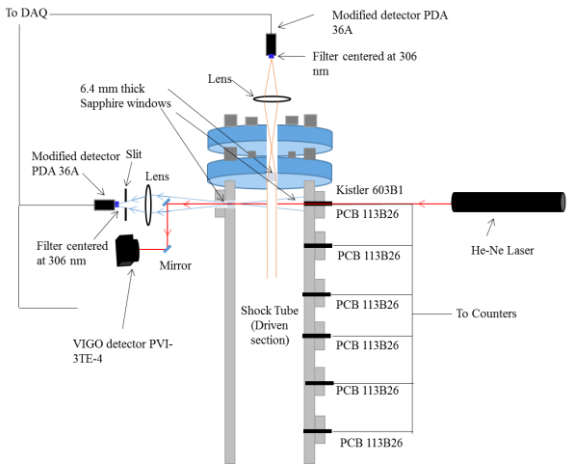

Figure 1. Experimental setup of the high-pressure shock tube (He-Ne laser beam and OH* emission signal are monitored from the same axial location but through different radial accesses)

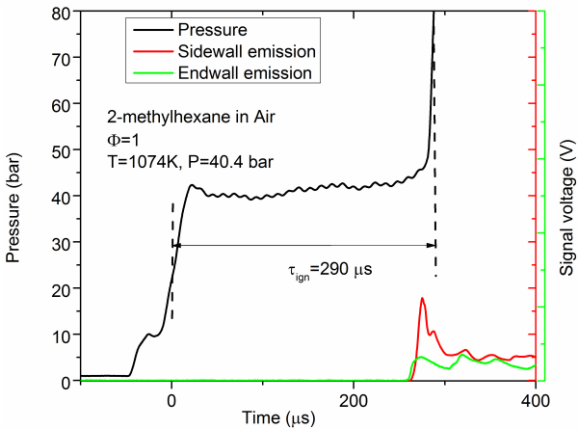

Figure 2. Typical pressure and OH* traces for single stage 2-methylhexane ignition

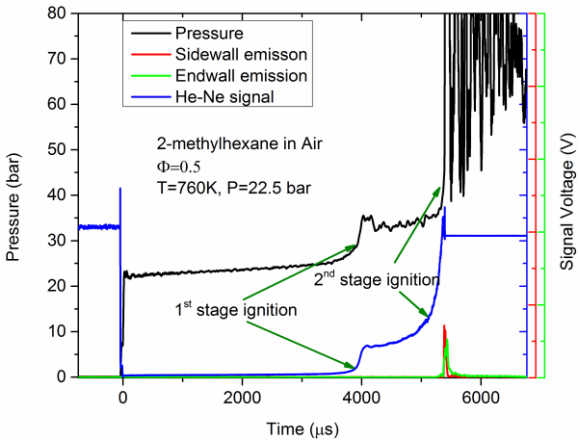

Figure 3. Typical pressure, He-Ne laser and OH* traces for two-stage 2-methylhexane ignition

2.2 Rapid compression machine measurements

For conditions resulting in ignition delay times longer than 2 ms, ignition delay time measurements were carried out in a rapid compression machine (RCM) at NUI Galway. The RCM is an experimental platform designed to promptly compress a test gas to an elevated temperature and pressure in order to probe chemical kinetic processes of the gas at the elevated thermodynamic state. The design of the machine and the method of ignition delay measurement using this device has been previously documented[25-28], and will not be further described here.

Ignition delay times were measured in the RCM at stoichiometric and fuel-lean (φ = 0.5) conditions in a bath gas containing 21% O_2 and 79% diluent. Experiments were conducted at compressed pressures of 20 and 40 bar (measured to ± 1%) in the compressed temperature range of 620–750 K. The test fuel 2-methylhexane was supplied in high purity (> 99%) by TCI UK, and used without further purification. Nitrogen (99.95%), oxygen (99.5%) and carbon dioxide (99.5%) gases were supplied by BOC Ireland. These experiments were mostly conducted using pure nitrogen diluent. However, to lower the specific heat ratio (i.e. γ = Cp/Cv) of the test gas and consequently provide access to lower compressed temperatures, a diluent mixture of 45% N_2 and 55% CO_2 was used for the fuel-lean experiments at compressed temperatures below 670 K. Experiments with stoichiometric mixtures compressed to 40 bar could not be performed in the RCM due to the high rate of heat release during ignition, which can cause damage to the dynamic pressure transducer (Kistler 6045a) used to monitor the pressure.

The RCM ignition delay measurements reported by Silke et al.[20] at φ = 1.0, at compressed pressures of 15 bar, and in the compressed temperature range of 630–925 K have also been reassessed here. For these experiments, a bath gas of 21% O_2 and 79% diluent was used. Pure

nitrogen was used as diluent for compressed temperatures below 750 K, while an 80% Ar / 20% N_2 diluent blend was used for higher temperatures to raise the specific heat ratio of the test gas and avoid excessive pre-heating of the machine. In the current study, 2-methylhexane was found to be highly reactive at these conditions with significant heat release during the compression process for compressed temperatures above 730 K making adequate comparisons between experimental and mechanism simulation results challenging. This has been alleviated by measuring ignition delay times at a slightly less reactive condition (i.e. Pc = 10 bar ±1%).

Ignition delay times are reported here as a function of the measured compressed pressure and mixture composition together with the compressed gas temperature, which is evaluated using the widely validated adiabatic core model[29-31]. Comparisons between the 2-methylhexane oxidation mechanism and RCM experiments are achieved by simulating the adiabatic core gas in a zero dimensional closed adiabatic reactor, where the reactor gas is volumetrically compressed or expanded at an empirically derived rate to account for the effects of piston compression and heat loss from the test gas to the reaction chamber surfaces, respectively.

3. Chemical kinetic model development

In this work, we updated the low- and high-temperature 2-methylhexane oxidation mechanism proposed by Sarathy et al.[18]. The C_0–C_4 base chemistry was replaced with the AramcoMech 1.4[32] base chemistry. Thermodynamic properties of chemical species were recalculated using updated group values. Furthermore, the rate coefficients of important low-temperature reaction classes were revised based on recent experimental and theoretical kinetic studies. Finally, alternative isomerization pathways of OOQOOH intermediates were added to the mechanism. These updates are discussed in detail in subsequent sections. All simulations were conducted using the

homogeneous batch reactor model in CHEMKIN PRO[33], and thermochemical data were calculated using THERM software[34].

3.1 Updates of thermochemical data

The accuracy of thermochemical data is important in combustion modeling. Thermodynamic properties (heat of formation ΔH_f, entropy ΔS, and specific heat C_p) are used to estimate heat of reaction, equilibrium constants, and rates of reverse reactions. In this work, thermodynamic data is estimated using THERM software[34], based on the group additivity method (GA) proposed by Benson and co-workers [35]. This method divides the molecule into groups, each having its own contribution to thermodynamic properties. Typically, one can obtain properties within 0.96 kcal/mol chemical accuracy[36]. A second order estimation method is also used, in which corrections for 1,4 and 1,5 interactions, optical isomers, cyclization, etc. are accounted for[34].

In this work, updated ALPEROX ($OO^{\cdot}$ radical) and OO/C/H group values from Burke et al.[15] are used to recalculate the thermodynamic data of all species in the 2-methylhexane kinetic mechanism. Optical isomers and the effect of the non-next-nearest neighbor interactions (NNI), especially gauche interactions[36-37] were taken into account.

Optical isomers: An optical isomer (OI) group value is added for every chiral center in a chemical species. For example, a primary radical at C1 in 2-methylhexane (Figure 4) renders C_2 a chiral center as it is connected to four different groups, which requires the addition of the OI group value. It is also added for every OO and OOH group in peroxy and alkyl hydroperoxide species since they are considered as pseudo-chiral centers[11]. The OI group value adds a correction of Rln(2) to the entropy.

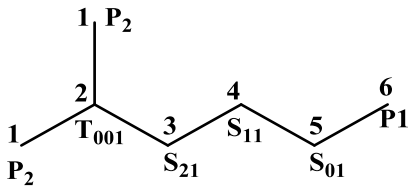

Figure 4. 2-methylhexane structure with labels to denote specific sites

Gauche interactions: In this work, three different types of gauche interactions are accounted for:

• Alkane gauche interaction (AG) is the classical gauche interaction[3] that occurs whenever a 60^{o} dihedral angle is formed between two carbons, as shown in Figure 5a. This destabilizes the energy by 0.8 kcal/mol[36]. Table 2 presents the counting scheme for gauche interactions based on the type of bond between the two central carbons. This scheme was revised by Cohen and Benson[38] in 1992 to better match the experimental enthalpies of highly substituted molecules (Table 2). In 2-methylhexane a tertiary and a secondary sites are adjacent, i.e. C_2 and C_3 in Figure 4, so one AG interaction is added.

• Radical gauche 1 interaction (RG1), of the same magnitude as AG, is considered when a radical site exists at one of the central carbons, as shown in Figure 5b. In this case, the radical is neglected and the revised counting scheme in Table 2 is used. For 2-methylhexane, C_2 and C_3 radicals are considered to have one gauche interaction[36-37].

• Radical gauche 2 interaction (RG2) is considered when a radical exists on sites neighboring the central carbons. In such cases, the molecule should be rearranged so as to minimize the number of AG interactions in favor of RG2 interactions (Figure 5c), since the destabilizing magnitude of the latter (0.4 kcal/mol) is less important. Considering that only one gauche interaction group value, corresponding to AG, exists in THERM databases, the RG2 interaction was neglected in this study. Therefore, RG2 interactions are not taken into consideration when calculating the thermodynamic properties of radical species. For example, no gauche effect is

assumed for the radical species in Figure 5c which has zero AG, zero RG1 and one RG2 interactions.

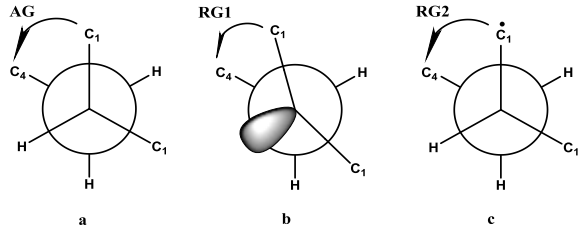

Figure 5. Newman projection of 2-methylbutane or C2-C3 bond in 2-methylhexane, a. gauche interaction, b. radical gauche 1, c. radical gauche 2

Table 2: Number of gauche interaction correction in classical and revised counting scheme[36]

Bond	Classical [35]	Revised [38]
P-P, S, T or Q	0	0
S-S	0	0
S-T	1	1
S-Q	2	2
T-T	2	3
T-Q	4	5
Q-Q	6	8

Table 3 shows a comparison between the original and updated thermodynamic properties of two low temperature species. These updates alter the thermochemical properties of low temperature species, which alters the equilibrium constants and reverse rates of some elementary reactions and ultimately influences reactivity. In the case of 2-methylhexane, as shown in the example in Table 3, the thermodynamic updates increases the Gibbs energy of the reaction which increases the reverse rate and shift the equilibria towards the reactants. This results in a reduced reactivity in the negative temperature coefficient (NTC) region as shown in Figure 6.

Table 3: A comparison of the thermodynamic properties using original and updated group values

			H (kcal/mol)	S (cal/(mol.K))	ΔG (kcal/(mol.K))	k_rev (sec^{-1})
c7h15oo-3-2		Original	–38.46	115.5		
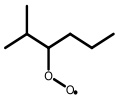		Updated	–35.86	116.8		
		Δ	+2.6	+1.3		
c7ooh3-2d		Original	–25.51	121.1		
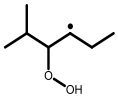		Updated	–22.68	120.4		
		Δ	+2.83	–0.7		
$RO_2 \rightarrow QOOH$	(298 K)	Original Δ	12.95	5.6	11.28	1.53
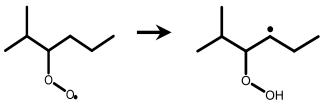		Updated Δ	13.18	3.6	12.12	6.30
	(800 K)	Original Δ	13.29	6.21	8.32	2.233E+06
		Updated Δ	13.14	3.50	10.34	7.936E+06

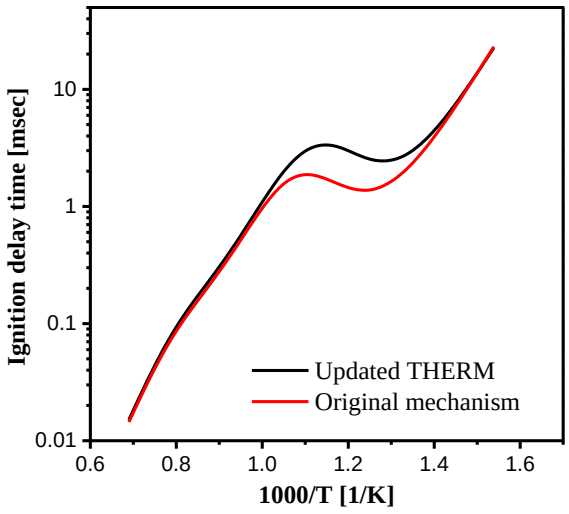

Figure 6. Constant volume simulated ignition delay profiles for 2-methylhexane/air mixtures at 40 bar, φ =1 using the original and updated thermodynamic data.

3.2 Updates to existing pathways

The detailed chemical kinetic mechanism describes the low- and high-temperature reactions that take place during fuel oxidation. Reactions are initiated by H-atom abstraction from the fuel forming fuel radicals that mainly undergo β-scission reactions leading to olefins and radicals at high temperature. At low temperatures, fuel radicals react with O_2 to form chemically activated alkylperoxy adducts (RO_2*). These adducts are collisionally stabilized at high pressure, leading to thermally equilibrated (RO_2) radicals. Both, chemically activated and thermally equilibrated adducts, undergo isomerization and concerted elimination reactions to form hydroperoxyalkyl radicals (QOOH) and olefins + HO_2, respectively (Figure 7). The concerted elimination pathway is a chain termination pathway that inhibits reactivity. Meanwhile, QOOH radicals undergo chain branching reactions upon the addition of molecular oxygen, ultimately leading to the formation of two reactive OH radicals, which promotes reactivity. Alternative isomerizations of the OOQOOH radicals (as discussed later) may also influence low temperature reactivity and ignition depending on the molecular structure and combustion conditions (i.e., temperature, pressure, equivalence ratio). QOOH radicals also undergo chain propagation and chain termination reactions leading to cyclic ethers + OH and olefins + HO_2, respectively. Competition of HO_2 elimination and cyclic ether formation with the second O_2 addition is partially responsible for the NTC behavior in 2-methylhexane ignition.

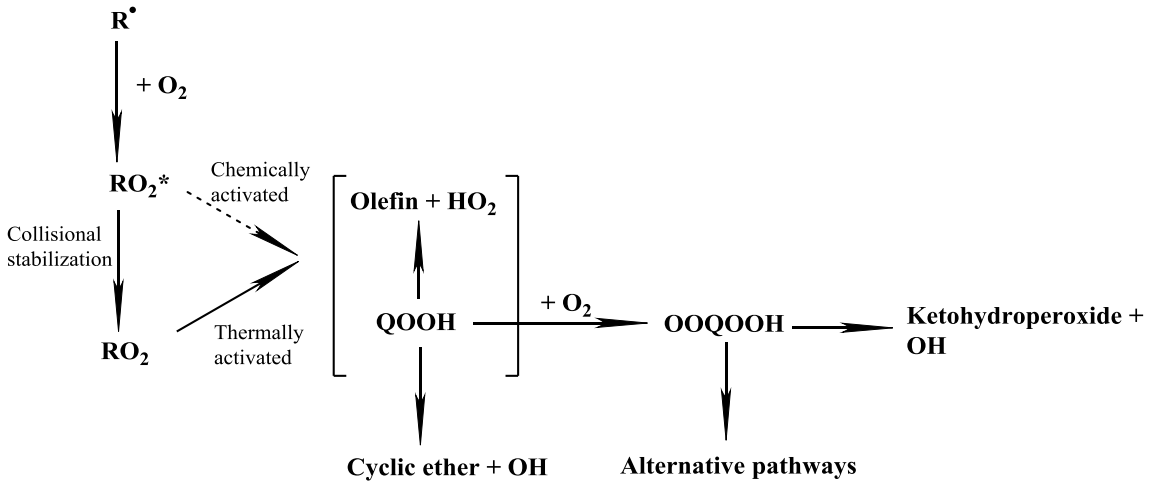

Figure 7. Schematic of low temperature pathways of hydrocarbon combustion

Several important reaction classes in the aforementioned reaction scheme have been revised and modified based on recent experimental and theoretical studies. High-pressure limit rate constants were revised based on recent quantum calculations using the same approach as Bugler et al.[5] and Zhang et al.[6] for the pentane isomers and *n*-hexane, respectively. Bugler et al.[5] also compared rate constants from different studies and provided a recommended set of rate coefficients with uncertainty bounds. We will later show how these recommended rate coefficients and their uncertainty bounds can be used for model optimization. High-pressure limit rate constants were used as Villano et al.[11], Goldsmith et al.[39], and Bugler et al.[5] concluded that high pressure limit rates are suitable for a typical combustion conditions (10 atm). They observed a small difference in concentrations and ignition when pressure dependent rates are used and this effect decreases as the molecule size increases.

After having updated the base C_0–C_4 chemistry [32] and the thermodynamic data of all chemical species, as described earlier, updates were made to the rate coefficients of the following reaction classes. The updates were incorporated sequentially, and simulations were performed after each update to monitor its effect on the kinetic model's reactivity. For example, the 7th update

comprises the update of QOOH + O_2 rate coefficients, in addition to the updates 1 through 6, as well as updates of the base chemistry and thermodynamic data.

1. (R + OH ↔ R$^{\cdot}$)
2. (1+(R$^{\cdot}$+ O_2 ↔ RO_2))
3. (2+(RO_2↔ QOOH))
4. (3+(RO_2 ↔ olefin + HO_2))
5. (4+(QOOH ↔ cyclic ether + OH))
6. (5+(QOOH ↔ olefin + HO_2))
7. (6+(QOOH + O_2 ↔ OOQOOH))
8. (7+(OOQOOH ↔ ketohydroperoxide +OH))
9. (8+(ketohydroperoxide decomposition))

3.2.1 Update 1: H-atom abstraction from the fuel by OH

Fuel abstraction by OH is important in fuel consumption at all temperatures. This class of reactions recently received attention from Sivaramakrishnan et al.[40] and Badra et al.[41], wherein experimental measurements of the rate of OH abstraction were made using the reflected shock tube technique. Both studies extend their measurements to quantify the effect of the next-nearest-neighbor (NNN) proposed by Cohen[42].

The NNN method differentiates between various primary, secondary and tertiary sites by considering the number of carbon atoms bonded to the carbon adjacent to the C–H site of interest. P0, P1, P2 and P3 are primary sites in which the carbon next to the C–H carbon is bonded to 0, 1, 2, or 3 other carbon atoms. Similarly, it is possible to differentiate between ten secondary sites, S_{ij}, where i and j are the number of other carbon atoms bonded to the two

carbons adjacent to the secondary site. For tertiary site, twenty different types T_{ijk} can be distinguished[40].

Based on the NNN method, Cohen[42] proposes a unique set of rate coefficients for each type of C–H site. The subscripts in Figure 4 show the NNN notation for each site. In this study, the rate coefficients of P1, P2, S01, and S11 are taken from Sivaramakrishnan et al.[40] while those of S21 and T001 are taken from Badra et al.[41] as they were not measured by Sivaramakrishnan et al.[40].

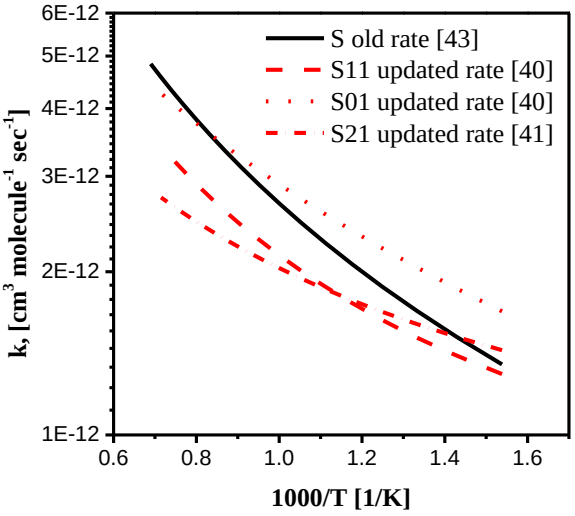

Figure 8 compares the rate constants of H-abstraction by OH for different secondary sites with those used in the original mechanism[43]. At intermediate temperatures, where abstraction by OH is more dominant, the rates differ by around ±15% from the original rate. The updates to the H-

abstraction reaction class result in a very minor effect, almost negligible, on the ignition delay time, as shown in Figure 9.

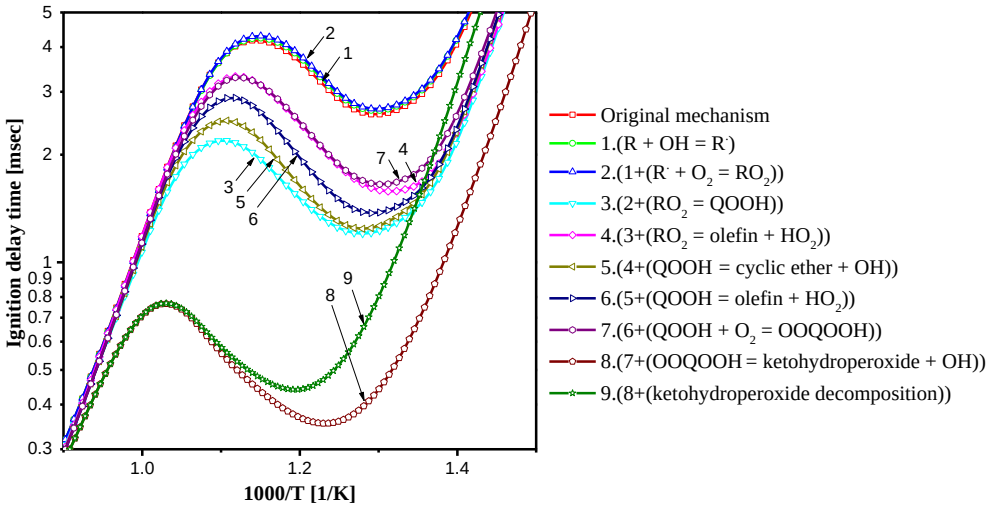

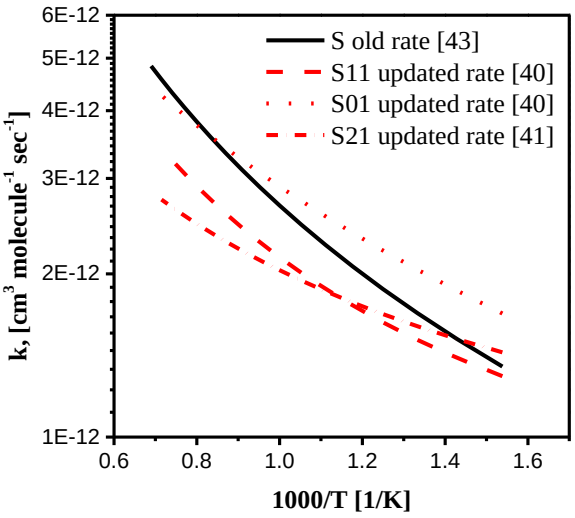

Figure 8. Site specific rate comparisons of H-atom abstraction by OH radical.

3.2.2 Updates 2 and 7: Addition of O_2 to alkyl radicals ($R^{\cdot} + O_2 = RO_2$) and Addition of O_2 to QOOH ($QOOH + O_2 = OOQOOH$)

The $R^{\cdot} + O_2$ reaction initiates the low temperature oxidation mechanism. The second O_2 addition to QOOH intermediates initiates low temperature chain branching. Miyoshi[12] calculated high-pressure-limit rate coefficients for the $R^{\cdot} + O_2$ reaction using variational transition-state

theory at the CBS-QB3//B3LYP/CBSB7 level of theory. Goldsmith et al. [39] computed the rate coefficients of propyl/isopropyl + O_2 and the corresponding QOOH + O_2 reactions using variable reaction coordinate-transition state theory (VRC-TST). Their results show that the rate of $R^{\cdot} + O_2$ is twice faster than that of QOOH + O_2. Bugler at al[5] compared ignition delay times obtained using Miyoshi[12] and Goldsmith et al. [39] rate rules for both 1st and 2nd O_2 additions. Better agreement with experimental data was found when Miyoshi's rate coefficients were used, with the A coefficient reduced by a factor of two for the 2nd O_2 addition, as per Goldsmith's findings. In this study, we utilized Miyoshi's[12] rate rule for $R^{\cdot} + O_2$ reactions and their rate constants were divided by two for QOOH + O_2 reactions.

3.2.3 Updates 3 and 4: Alkyl peroxy radical isomerization (RO_2 = QOOH) and Concerted eliminations (RO_2 = olefin + HO_2)

Villano et al.[11], Miyoshi[12], and Sharma et al.[10] calculated the rate constants of RO_2 isomerization. Bugler at al. [5] compared the values from these studies and showed discrepancies within a factor of 2-3. However, these differences had no effect on ignition delay times. In this work, Villano et al.'s[11] rate coefficients were used. These coefficients were calculated at the CCSD(T)/6-31+G(d')//B3LYP/6-311G(d,p) and the MP4(SDQ)/6-31G+(d,p)//B3LYP/6-311G(d,p) levels of theory. Transition state theory was used to determine high-pressure limit rate coefficients for reactions involving C_1-C_5 and few selected C_6 and C_7 alkyl peroxy radicals.

In this study, alkyl peroxy to alkyl hydroperoxy isomerization reactions proceeding via 5-, 6-, 7- and 8- membered ring transition states (TS) were considered. The rates of these reactions depend on the TS ring size and the type of hydrogen being abstracted, where abstraction from primary is more difficult than abstraction from secondary, which in turn is more difficult than abstraction from tertiary. They also depend on the position of the abstracted hydrogen relative to

the peroxy group (α, β, γ, δ, or ε). Villano et al.[11] take these parameters into account when calculating the rate coefficients of isomerization reactions and thus, their values were used in our mechanism.

The concerted elimination reaction of RO_2 is an endothermic reaction that forms HO_2 radicals which are not highly reactive[5, 44]. Villano et al.[11] found that the activation energy of this elimination reaction is hardly affected by the thermochemistry or the bond dissociation energies of C–OO and C–H bonds. The reactivity of this pathway is only influenced by the chemical nature of the produced olefin. The rates are 2 to 3 times faster if highly substituted olefins are formed [11]. In this work, we used the rate coefficients for the less substituted olefins.

3.2.4 Update 5: Cyclic ether formation (QOOH = cyclic ether + OH)

This reaction class was updated based on the computational study of Villano et al.[13] that relates the activation energy of cyclic ether formation reactions to the degree of reaction exothermicity. These relations depend on ring size and the level of substitution. Based on their findings, Villano et al.[13] propose an equation that describes the relationship between activation energy and reaction enthalpy at 298 ^{o}C. The proposed equation is used along with updated thermochemistry data to estimate the activation energy and rate coefficients of cyclic ether formation reactions in this study.

3.2.5 Update 6: QOOH = olefin + HO_2 (radical site β to OOH group)

This reaction is basically a *β*-scission of the C–OOH bond in alkyl hydroperoxy species where the radical site is located at *β*-position relative to the OOH group. Villano et al.[14] calculated the high-pressure-limit rate coefficients of these reactions, in the reverse, exothermic direction, for C_2–C_5 and selected C_6 and C_7 olefins at the same level of theory used in their previous work[11, 13].

They showed that the entropy of HO_2 addition depends on the level of substitution, and that the activation energy depends on the nature of the *β*-carbon (primary, secondary or tertiary).

3.2.6 Update 8: Isomerization of OOQOOH (OOQOOH ↔ ketohydroperoxide + OH)

Peroxy-alkylhydroperoxide (OOQOOH) radicals isomerize via migration of the most weakly bound hydrogen at the *α*-site to the hydroperoxide group. This migration is quickly followed by *β*-scission reactions to form an OH radical and a ketohydroperoxide. The weak O–OH bond in the ketohydroperoxide then breaks to form OH and an alkoxy radical. This sequence of chain branching reactions is responsible for low-temperature reactivity[10].

In the original mechanism which was developed based on Curran et al.[19], the rate coefficients used for ketohydroperoxide formation were assumed to be the same as those of RO_2 isomerization with an activation energy correction of 3 kcal/mol to account for the weaker C-H bond α to the OOH moiety. However, Sharma et al.[10] found that the difference between the activation energies of RO_2 isomerization and OOQOOH isomerization varies with the transition state's ring size. They estimated corrections of 8.6, 2.2 and 0 kcal/mol for 5-, 6- and 7-membered ring migrations, respectively. Both, Miyoshi[12] and Sharma et al.[10] calculated the rate coefficients for this reaction class. Bugler et al.[5] compared the rate constants of the two studies and investigated in detail the effect of implementing each set on the ignition delay time of pentane isomers. They showed that the use of Sharma's rate coefficients gives very good agreement with experimental ignition delay data, better than when using Miyoshi's rate coefficients. Therefore, values from Sharma et al.[10] were used in this work. These values are determined computationally at the CBS-QB3//B3LYP/6-31G(d) level of theory using coupled internal rotor treatment.

3.2.7 Update 9: Ketohydroperoxide decomposition

Ketohydroperoxide decomposition is the last step in the low temperature chain branching reaction sequence. A ketohydroperoxide species undergoes scission of the weak O–OH bond, thereby forming an alkoxy rapidly that further decomposes to smaller molecules through a series of β-scissions. Different rate rules and barriers have been suggested for this reaction class[8, 19]. The original model by Sarathy et al.[18] utilized an activation energy of 39 kcal/mol for ketohydroperoxide decomposition. Bugler at al.[5] and Zhang et al.[6] modified the activation energy to values which are closer to the one calculated by Jalan et al.[45] of 43 kcal/mol. In this study, the updated activation energy value of 42.3 kcal/mol from Zhang et al.[6] was adopted for this reaction class, as well as other O–OH scission (e.g. hydroperoxide cyclic ethers, olefinic-hydroperoxide, etc.).

Updating the rate constants of all the previously discussed updates from 1 to 9, resulted in a 85% reduction of ignition delay time as shown in

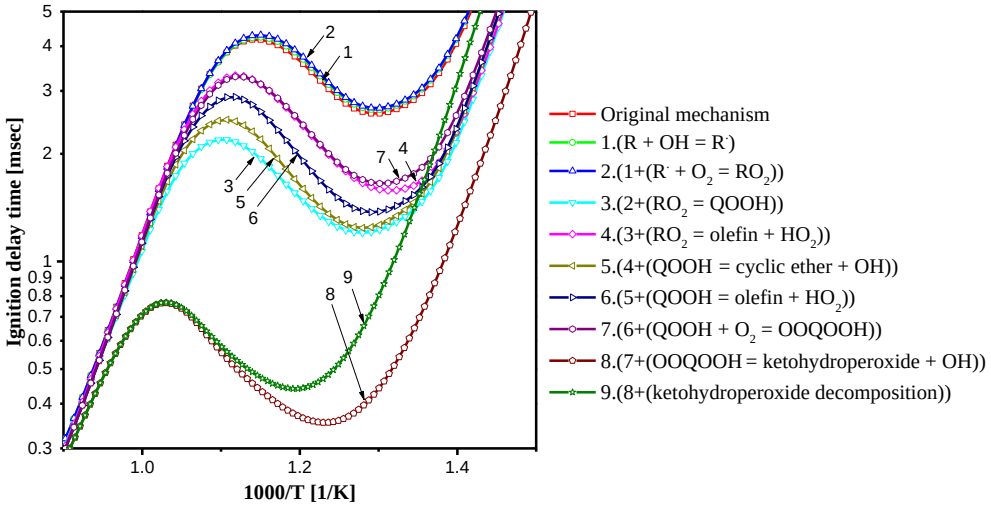

Figure 9. The major effect on reactivity resulted from updates (e.g. update 3 and 8) where the updated rates are significantly higher than the rates in the original mechanism. A comparison between the original and updated rate constants are shown in the supplementary material.

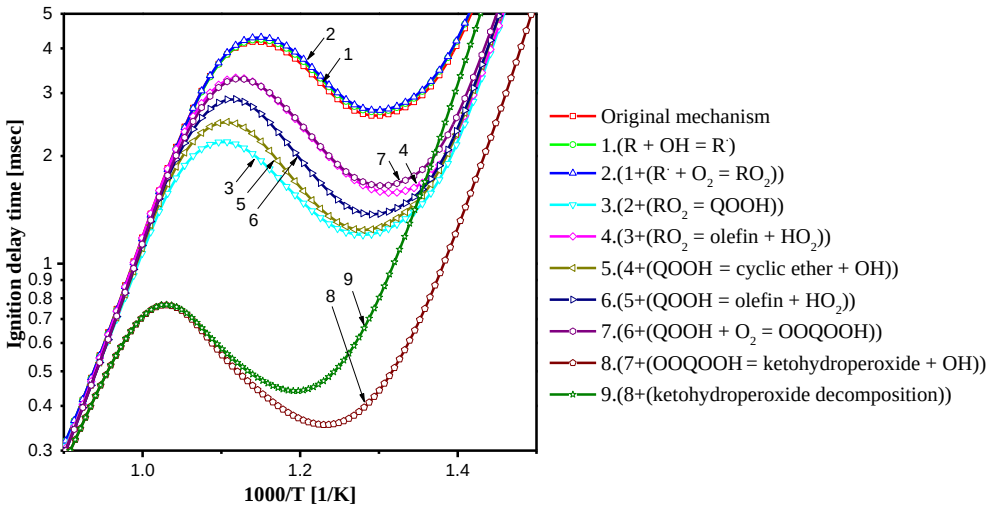

Figure 9. Constant volume simulated ignition delay time for 2-methylhexane/air mixtures at 40 bar, φ =1, using the original mechanism and updated thermodynamic data, base chemistry and reaction rate coefficients.

3.3 Addition of alternative isomerization pathways

In the original mechanism, only migration of the weakest hydrogen at the α-site to the peroxy group in OOQOOH was considered. This pathway leads to ketohydroperoxide and OH radical as discussed above. Alternatively, the peroxy group can abstract a hydrogen from other sites, leading to alkyldihydroperoxides $P(OOH)_2$. This specie can further decompose to form hydroperoxide cyclic ether + OH and olefinic-hydroperoxide + HO_2. Sharma et al.[10] mentioned the importance of these pathways and recommended more efforts to explore them. Silke et al.[7] included these pathways in the *n*-heptane mechanism developed originally by Curran et al.[8]. They found that including them leads to longer ignition delay due to the high concentration of the HO_2 radicals produced. However, the rate coefficients of these reactions were assigned based on analogy with QOOH reactions, which leads to a relatively high level of uncertainty. Bugler et al.[5] also considered these alternative pathways and their subsequent reactions and found that they

had little effect on reactivity. Figure 10 shows an example for the conventional and alternative OOQOOH isomerization pathways considered in this study.

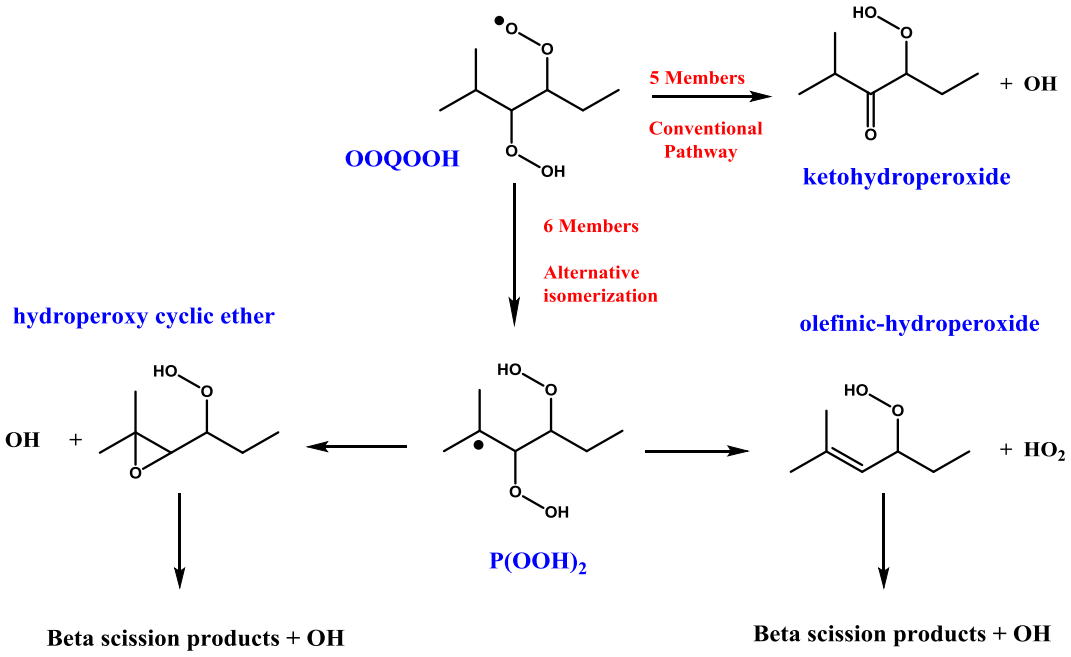

Figure 10. Schematic of conventional and alternative pathways of OOQOOH isomerization

3.3.1 $OOQOOH \leftrightarrow P\cdot(OOH)_2$

Figure 11a shows an example from the 2-methylhexane mechanism of the conventional isomerization pathway forming ketohydroperoxide and the alternative pathway of abstracting from a secondary carbon site. A rate comparison in Figure 11b shows that, for this particular case, the alternative pathway is faster by over an order of magnitude and is dominant over the pathway to ketohydroperoxide formation. The alternative pathway is favored for this specific radical because hydrogens bonded to the secondary site have a lower bond dissociation energy than hydrogens bonded to the primary site adjacent to the hyroperoxyl group. However, other OOQOOH radicals with different molecular structure still favor the ketohydroperoxide formation because alternative isomerization are not competitive. Only 6-member ring transition state for

alternative isomerizations and subsequent reactions are included in this work. This is due to the relatively low steric cost of forming 6-member rings that makes them more favorable. Since no rate rules are estimated for these reactions explicitly, functional group analogy was used to assign rate constants. Villano et al.'s[11] rate coefficients of RO_2 isomerization are used for this class.

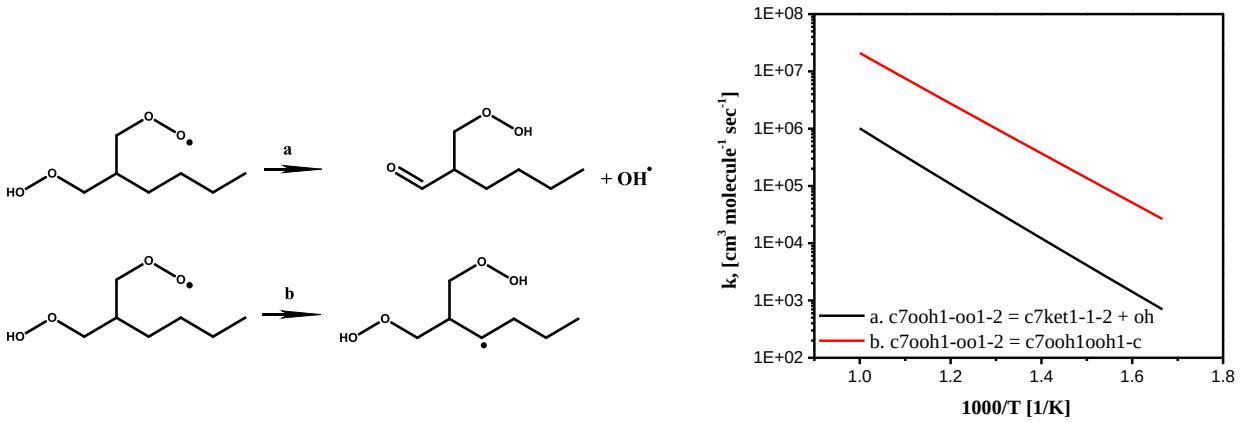

Figure 11. (a) Conventional and alternative pathways of OOQOOH. (b) rate constant comparison of conventional and alternative pathways

3.3.2 $P(OOH)_2$ ↔ olefinic-hydroperoxide+HO_2

This pathway is added in analogy to olefin production from QOOH using Villano et al.'s[14] rates for $P(OOH)_2$ species with a radical in the beta position relative to the OOH group. Silke et al.[7] argue that this chain termination pathway reduces reactivity when alternative pathways are added. However, further decomposition of olefinic-hydroperoxide by O–O scission of the OOH group will produce OH radicals. Therefore, an HO_2 and an OH radical are produced from $P(OOH)_2$ compared to two OH radicals from the conventional isomerization pathway. Considering that OH has a higher fuel abstraction potential than HO_2, the conventional isomerization pathway yields higher reactivity than the alternative one at low temperatures. However, at intermediate temperatures, HO_2 radicals are converted into two OH via the

dissociation of H_2O_2 intermediates, and thus, their production increases reactivity. This is consistent with the study of Bugler et al.[5] which showed that, in the case of pentane, the production of HO_2 and OH instead of two OH radicals reduces reactivity at low temperature and increases reactivity at intermediate temperatures. However, this reactivity trend was not observed in our study because hydroperoxy cyclic ether formation is more dominant as explained in the following section.

3.3.3 $P(OOH)_2$ ↔ hydroperoxide cyclic ether + OH

The rate coefficients for this reaction class are analogous to those taken from Villano et al. [13] for cyclic ether formation from QOOH. Hydroperoxide cyclic ether further decomposes via O–O scission of the hydroperoxide entity. Therefore, this pathway leads to the formation of two OH radicals. In this work, where only 6-membered ring alternative isomerizations are accounted for, the rate of producing hydroperoxide cyclic ether + OH from $P(OOH)_2$ is considerably higher than the production of olefinic-hydroperoxide + HO_2. This is due to the relatively low concentrations of $P(OOH)_2$ species with a β-positioned OOH that may undergo HO_2 elimination. Consequently, the effect of HO_2 in reducing reactivity is suppressed and an overall increase in reactivity is observed upon the addition of alternative isomerization pathways, over a wide temperature range, as shown in Figure 12.

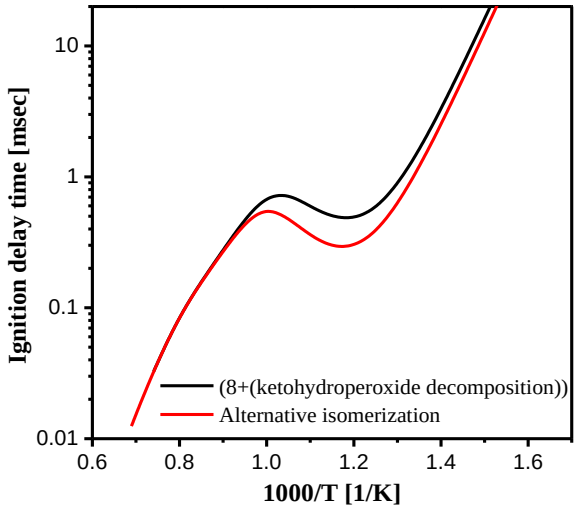

Figure 12. Effect of adding alternative isomerization pathways on ignition delay time of 2-methylhexane/air mixtures at 40 bar, φ =1.

4 Experimental and modeling results

The updated model is compared against new experimentally measured ignition delay profiles at 20 and 40 bar, stoichiometric and fuel-lean conditions, as shown in Figure 13. The thermodynamic and kinetic updates implemented, particularly the addition of alternative OOQOOH isomerization pathways, significantly affected the reactivity of the model. The experimental data at 20 and 40 bar indicate a transition to high temperature reactivity around 900 K for both fuel-lean and stoichiometric conditions. This transition out of the NTC and into the high temperature regime indicates a transition from fuel radical $R^{\cdot} + O_2$ chemistry to radical β-scission reactions. The kinetic model predicts the transition to high temperature reactivity at around 950 K, which is notably different than the experiments. Once in the high temperature regime, (e.g., above 950 K), the kinetic model accurately captures the experimental data at all conditions in Figure 13. The NTC regime in the experiments is generally in the range 800–900 K and is more pronounced at stoichiometric conditions compared to fuel-lean conditions. The kinetic model qualitatively captures the equivalence ratio dependence of the NTC regime;

however, ignition delay times are consistently under predicted in this regime (i.e., the model is too reactive). Below 800 K, the experiments depict typical Arrhenius-type low temperature reactivity, which is qualitatively captured by the model. First stage ignition delay times measured in the HPST are also presented in Figure 13, together with simulation results. The measured first stage ignition delay times indicate Arrhenius-type behavior and little pressure dependence at both lean and stoichiometric conditions, and the simulations qualitatively capture these features. However, both first stage and overall ignition delay times are quantitatively under predicted by the model in the low temperature regime.

In summary, the kinetic model under predicts ignition delay times in the low temperature and NTC regimes, which indicates deficiencies in the branching ratios of competing low temperature chain branching, propagation, and termination reactions. Considering that this discrepancy is most probably due to uncertainties in kinetic rate coefficient measurements or computations, these parameters were modified for some reaction classes in order to improve agreement between model and experiments. Two methods of modification were implemented. The first is a manual tuning that relies on manual manipulation of the rate coefficients of sensitive reactions. The second is automated optimization that relies on a model and experimental uncertainty quantification based on rigorous mathematical formulations.

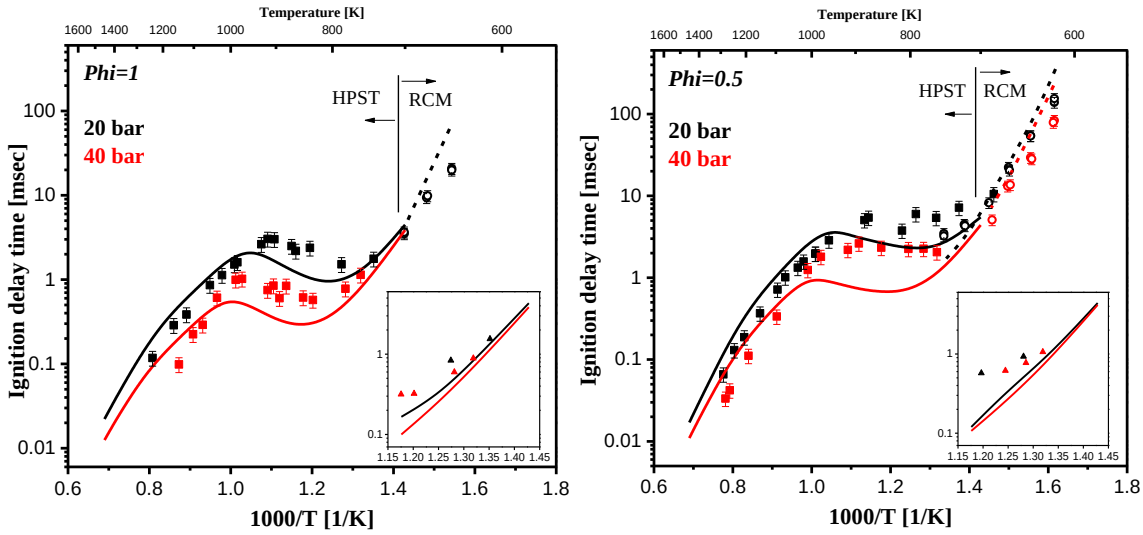

Figure 13. Updated model compared to HPST (solid line and square symbols) and RCM (dashed line and circle symbols) data. The insets illustrate 1st stage ignition measured in the HPST.

4.1 Sensitivity analysis and manual rate constant tuning

A brute force sensitivity analysis, implemented at φ =1 and 0.5, 40 bar and 800 K, is shown in Figure 14 (see Supplementary Material for a species dictionary). A temperature sensitivity analysis at the time of ignition was first conducted at the same conditions to determine the most sensitive reactions to be considered in the brute force sensitivity. Brute force sensitivity coefficients were calculated using the equation below, where τ_2 and $\tau_{0.5}$ are the ignition delay times estimated after multiplying the rate of the reaction by 2 and 0.5, respectively:

$$\sigma = \frac{\log(\tau_2 / \tau_{0.5})}{\log(2/0.5)}$$

A positive sensitivity indicates that increasing the rate of the reaction decreases reactivity and vice versa. Figure 14 shows that QOOH + O_2 and RO_2 isomerization pathways increase reactivity since these pathways lead to the formation of ketohydroperoxides and subsequent low temperature chain branching. Fuel abstraction by OH (except c7h15-2b (see Figure 4)) and the

chain branching reaction H_2O_2 (+M) ↔ OH + OH (+M) pathways also promote reactivity at the conditions investigated. Fuel abstraction form a tertiary site (c7h15-2b) showed a positive sensitivity because this radical will not form the reactive ketohydroperoxide and will only terminate through alternative pathways. This radical will react with O_2, isomerize and then form OOQOOH with hydroperoxide group in the tertiary site. As ketohydroperoxides are formed through the migration of the hydrogen at the α-site to the hydroperoxide group, this hydrogen is not available in the corresponding OOQOOH to c7h15-2b radical which terminates its contribution to the low temperature chemistry and decrease reactivity. A schematic shows the low temperature pathways of c7h15-2b (positive sensitivity) and c7h15-2d (negative sensitivity) is shown in the supplementary material. Chain propagation reactions of cyclic ether formation, precisely 5-member rings, and RO_2 concerted elimination have positive sensitivity coefficients, which means that they reduce reactivity. Base chemistry reactions that consume OH radical and reactions that form stable molecules decrease reactivity and thus have positive sensitivity coefficients.

The rate coefficients of selected low temperature reaction classes having high sensitivity coefficients have been modified within the uncertainty limits defined by Bugler at al.[5], as illustrated in Table 4. These modifications were consistently applied to all reactions within the same reaction class. The rates of 5-membered ring cyclic ether formation and O_2-addition to QOOH were multiplied and divide by 2, respectively. The ignition delay profiles simulated using

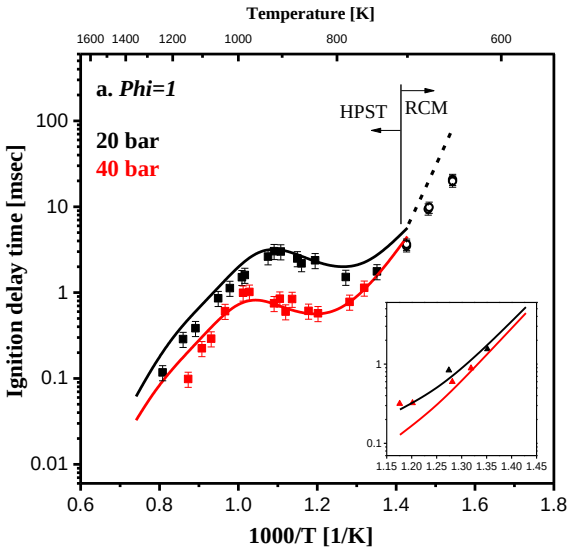

the tuned model are shown in

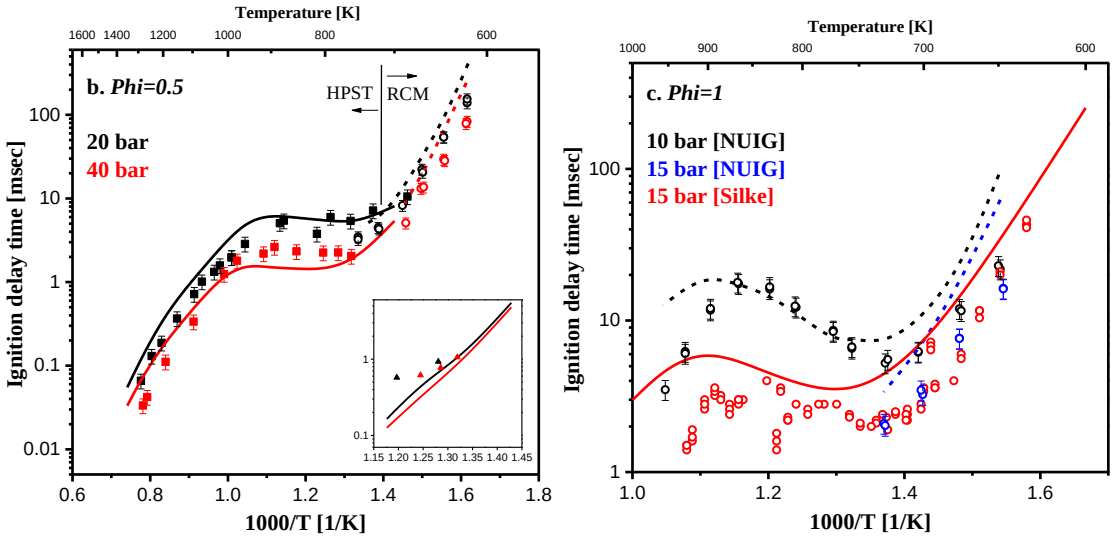

Figure 15.

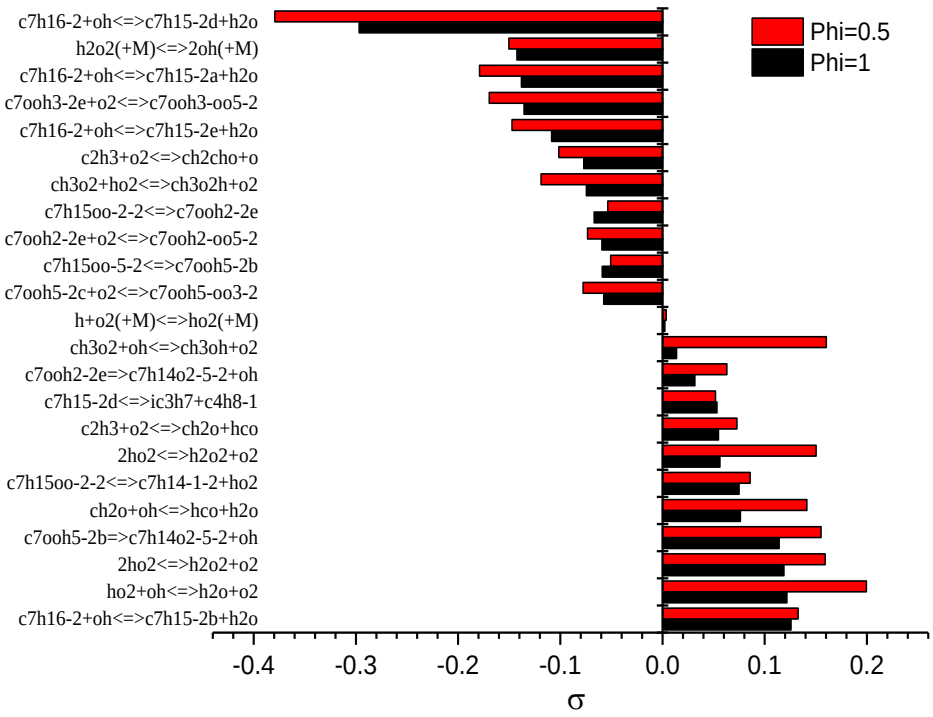

Figure 14. Brute force sensitivity analysis for ignition delay time at φ =1 and 0.5, 40 bar and 800K

The tuned model shows good agreement with the HPST data at the different conditions, and a better agreement with the first stage ignition delay time especially at $\boldsymbol{\varphi}$ =1, as illustrated in

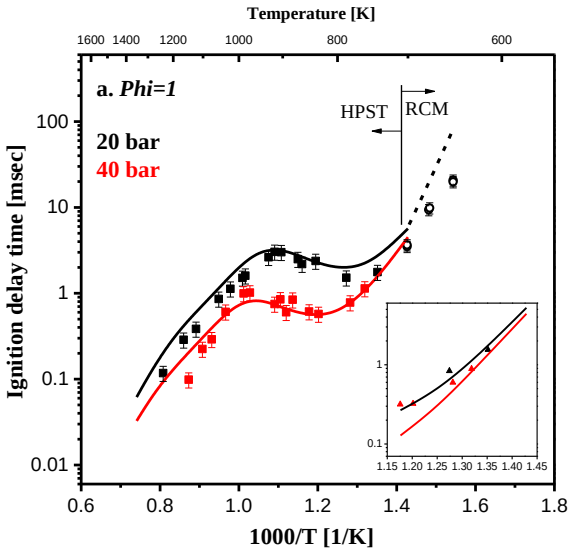
Temperature [K]
1600 1400 1200 1000 800 600
a. Phi=1
HPST
RCM
20 bar
40 bar
Ignition delay time [msec]
100
10
1
0.1
0.01
0.6 0.8 1.0 1.2 1.4 1.6 1.8
1000/T [1/K]
1.15 1.20 1.25 1.30 1.35 1.40 1.45

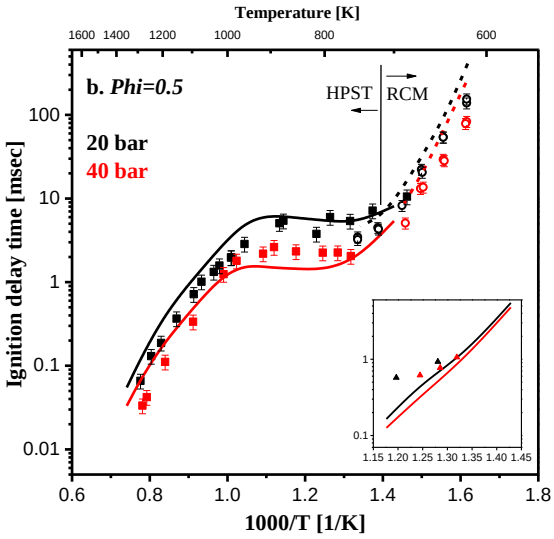
Temperature [K]
1600 1400 1200 1000 800 600
b. Phi=0.5
HPST
RCM
20 bar
40 bar
Ignition delay time [msec]
100
10
1
0.1
0.01
0.6 0.8 1.0 1.2 1.4 1.6 1.8
1000/T [1/K]
1.15 1.20 1.25 1.30 1.35 1.40 1.45

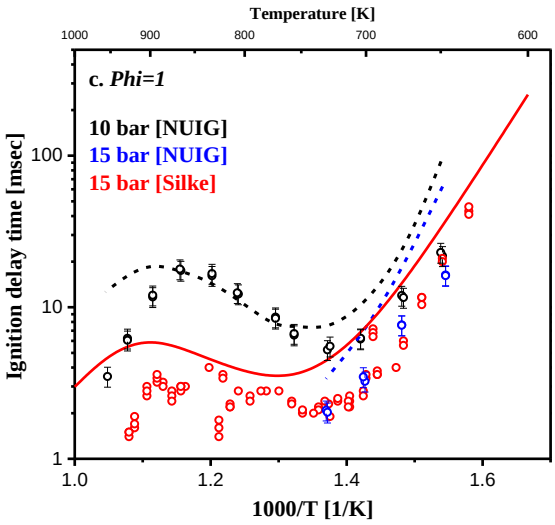
Temperature [K]
1000 900 800 700 600
c. Phi=1
10 bar [NUIG]
15 bar [NUIG]
15 bar [Silke]
Ignition delay time [msec]
100
10
1
1.0 1.2 1.4 1.6
1000/T [1/K]

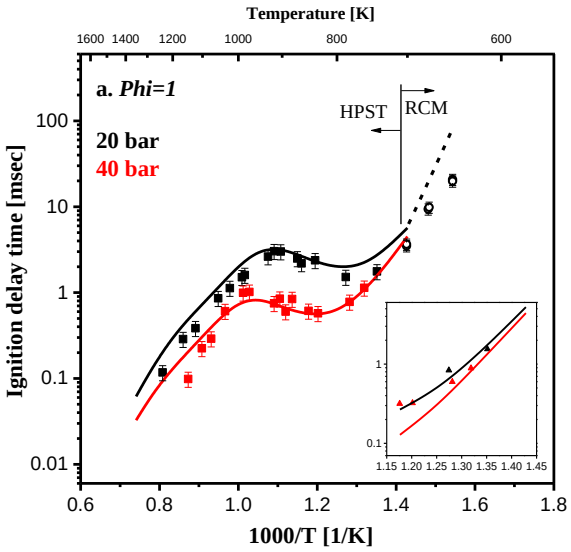

Figure 15a and

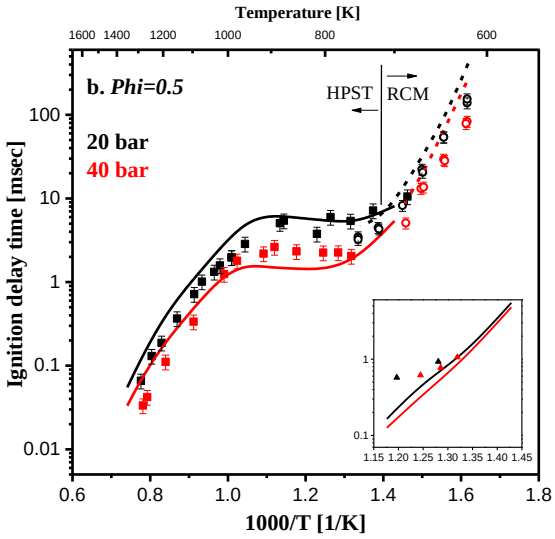

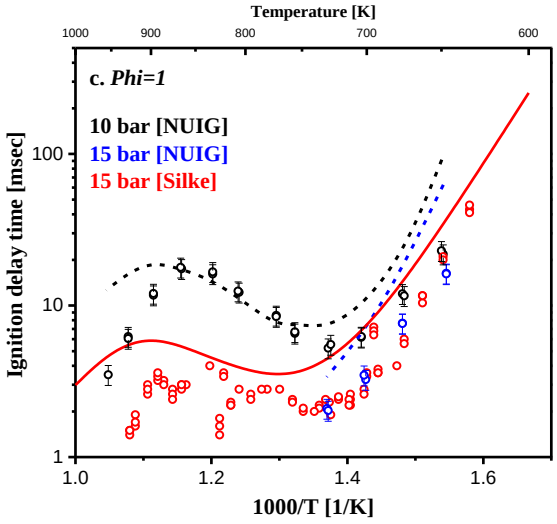

Figure 15b. The transition temperature between various reactivity regimes (low temperature, NTC, and high temperature) are accurately captured by the tuned model. The quantitative agreement in the NTC regime is also significantly better in the tuned model. These improvements are attributed to the applied modifications constraining the branching ratios of competing low temperature chain branching, propagation, and termination reactions. This was achieved by reducing the rates of OOQOOH formation and increasing the rates of the competing cyclic ether formation pathway. Figure 16 presents a flux analysis for 2-methylhexane oxidation

at 20 bar, intermediate temperature of 800 K, and a time corresponding to 20% fuel consumption. The branching ratio of QOOH in the tuned mechanism (**Bold %**) changed in the direction of favoring the cyclic ether formation over the 2nd O_2 addition compared to the updated (untuned) mechanism (*italic %*). The flux diagram also illustrates isomerization of the primary RO_2 radical and the subsequent major pathways leading to various chain branching, propagation, and termination pathways (e.g., cyclic ethers, ketohydroperoxides, and alkyldihydroperoxides ($P(OOH)_2$), etc.). The diagram shows that two of the three formed OOQOOH species favor the alternative isomerization pathway ($P(OOH)_2$), by 96% and 66% compared to 2% and 15% for the conventional pathway (ketohydroperoxide), respectively.

Table 4: Modification of the rate rules

Reaction class	Rate rule	Modification	Comment
5-member ring, Cyclic ether formation (QOOH = cyclic ether + OH)	Villano[13]	A*2	Also, 5m rings HPCE formation, ($P(OOH)_2$ = HPCE + OH)
Addition of O_2 to QOOH (QOOH + O_2 = OOQOOH)	Miyoshi[12]/2	(A/2)/2	Original rates divided by 2 based on Goldsmith et al. [39] recommendation

Longer ignition delay times at temperatures below 715 K were observed compared to the RCM experimental data at all pressures. This might refer to the less reactive kinetics at these low temperatures, and thus the rates for ketohydroperoxide decomposition (as well as hydroperoxide cyclic ether, olefinic-hydroperoxide and ROOH decomposition) needs to be revisited. Good agreement was found at temperatures higher than 730K at 10 bar (

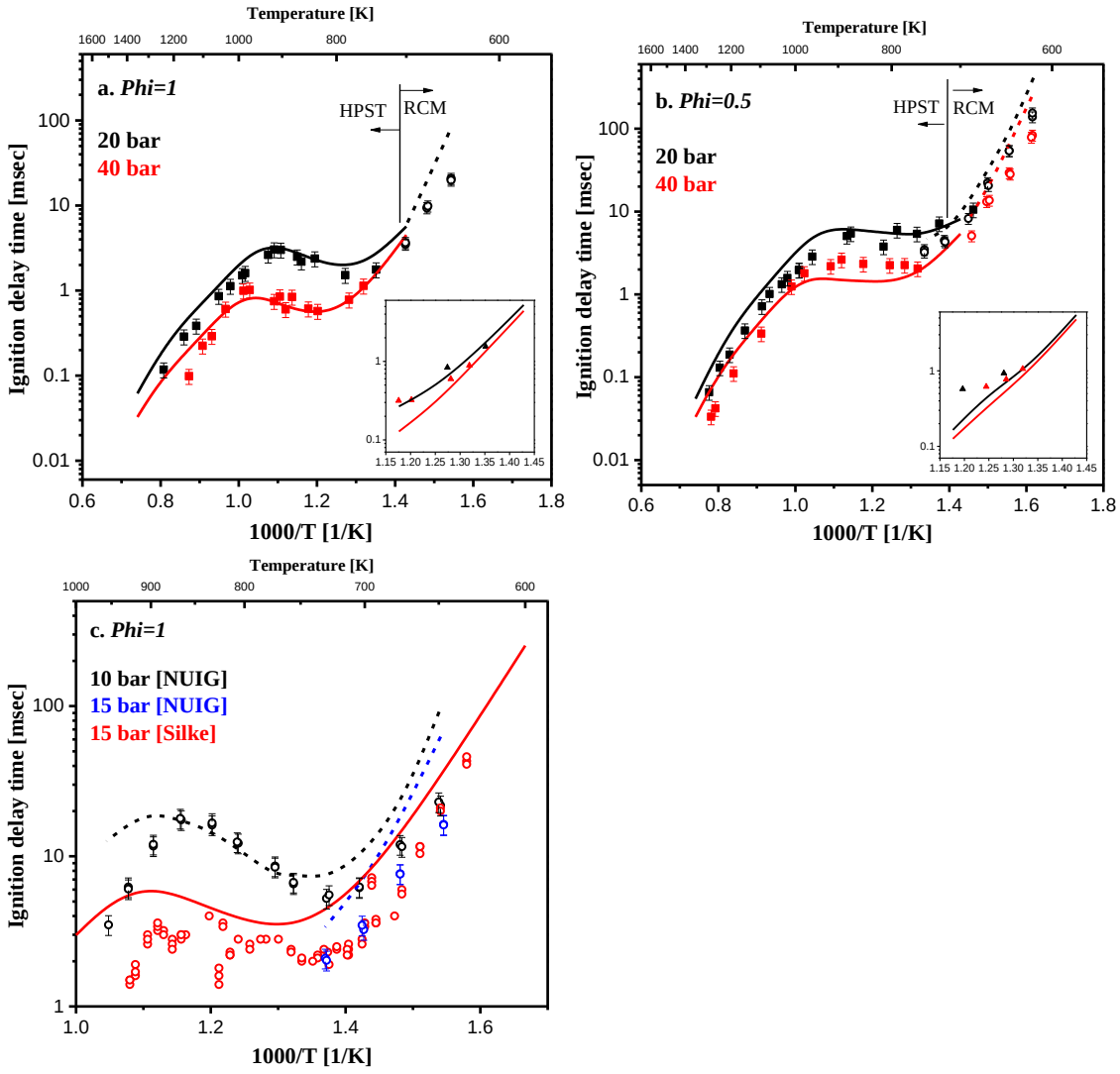

Figure 15c), whereas at higher pressures (20 bar, φ = 0.5) expected ignition delay times become very short, which is a difficult condition to obtain ignition delay measurements in an RCM as reactions might start to occur before the end of compression. When both shock tube and RCM data are available at the same condition, as shown in

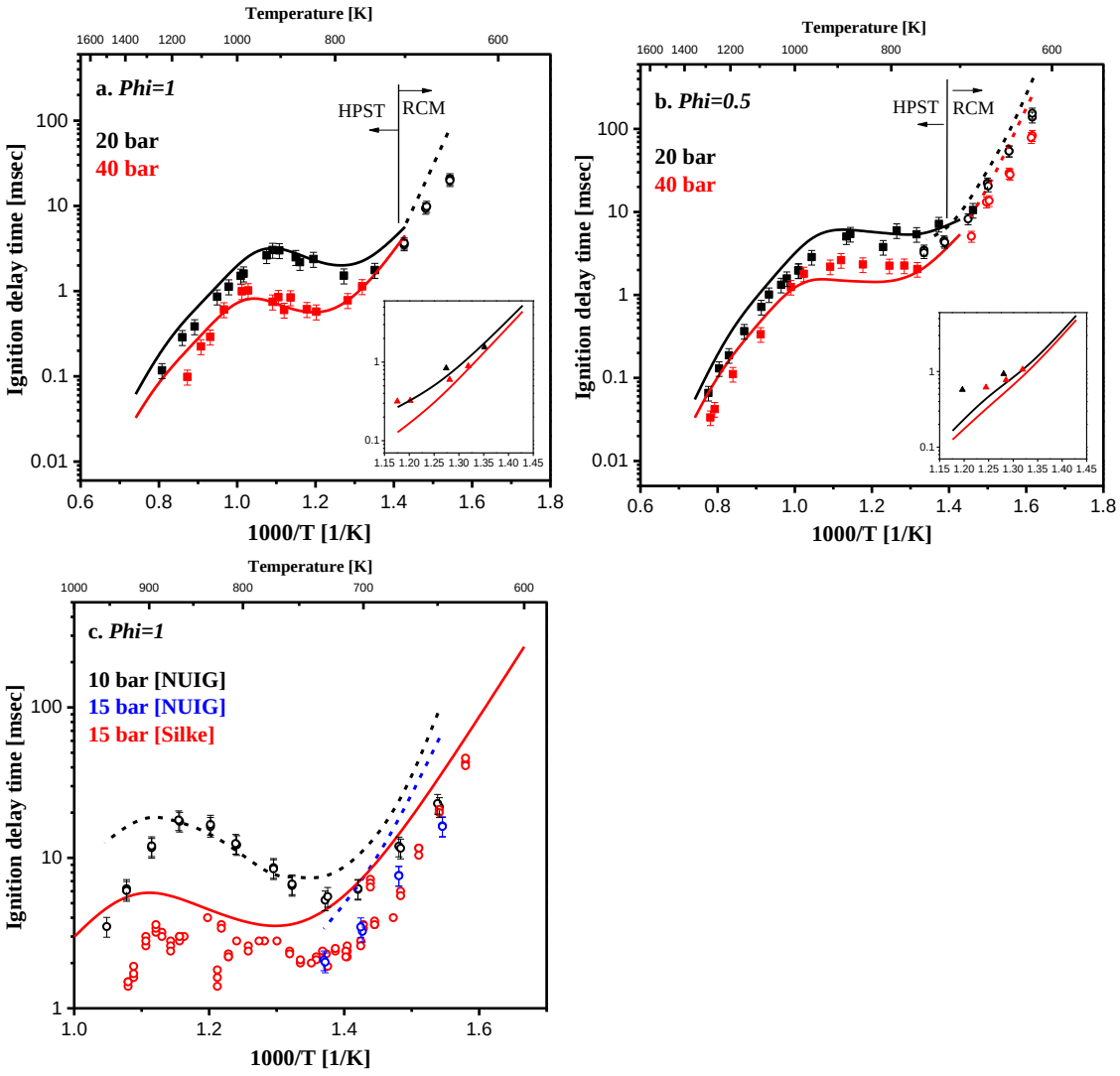

Figure 15b, the model better matches shock tube experiments in comparison to RCM experiments.

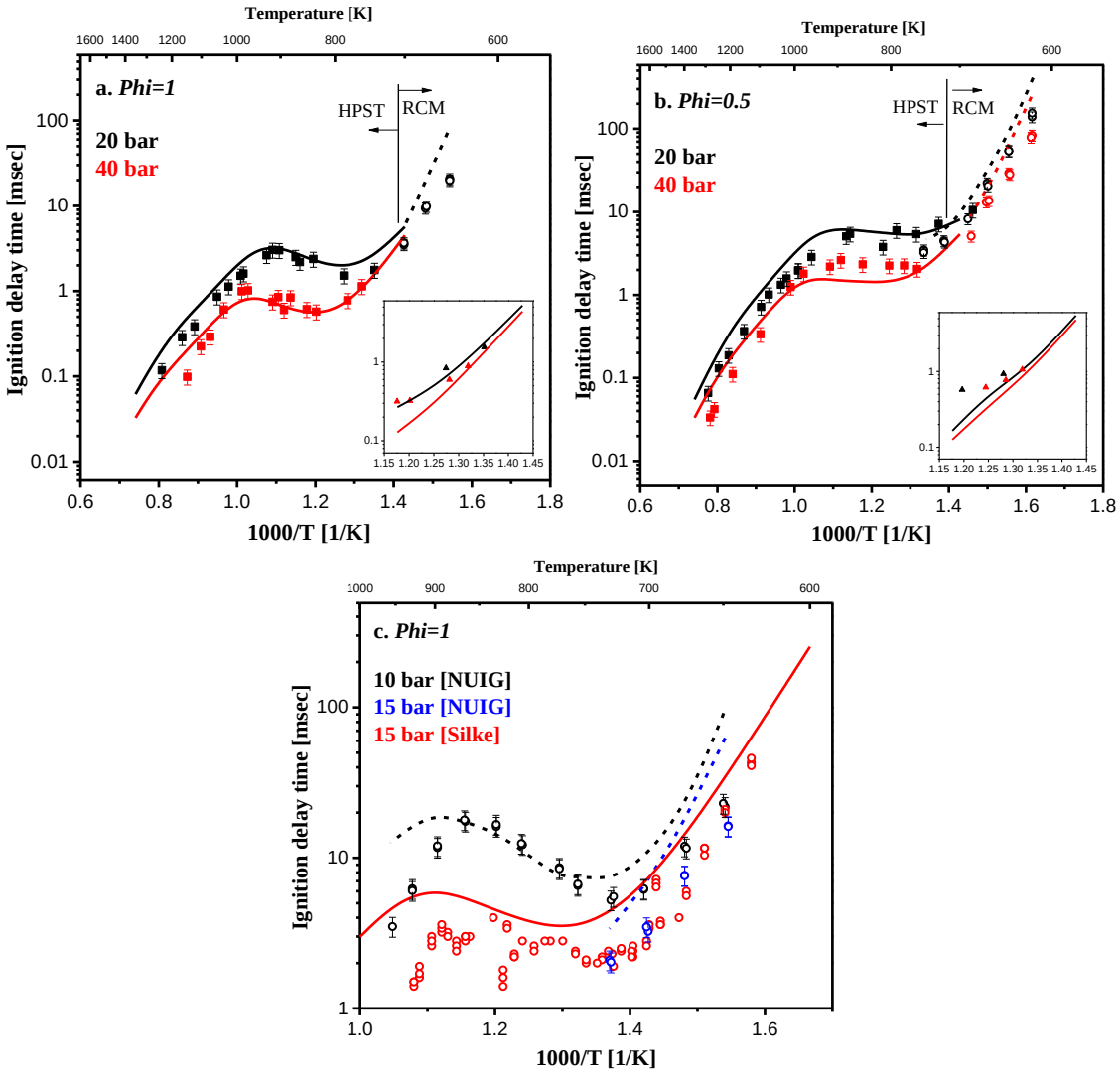

Figure 15. Final model after tuning compared to HPST (solid line and square symbols) and RCM (dashed line and circle symbols) data. The insets illustrate 1st stage ignition measured in the HPST.

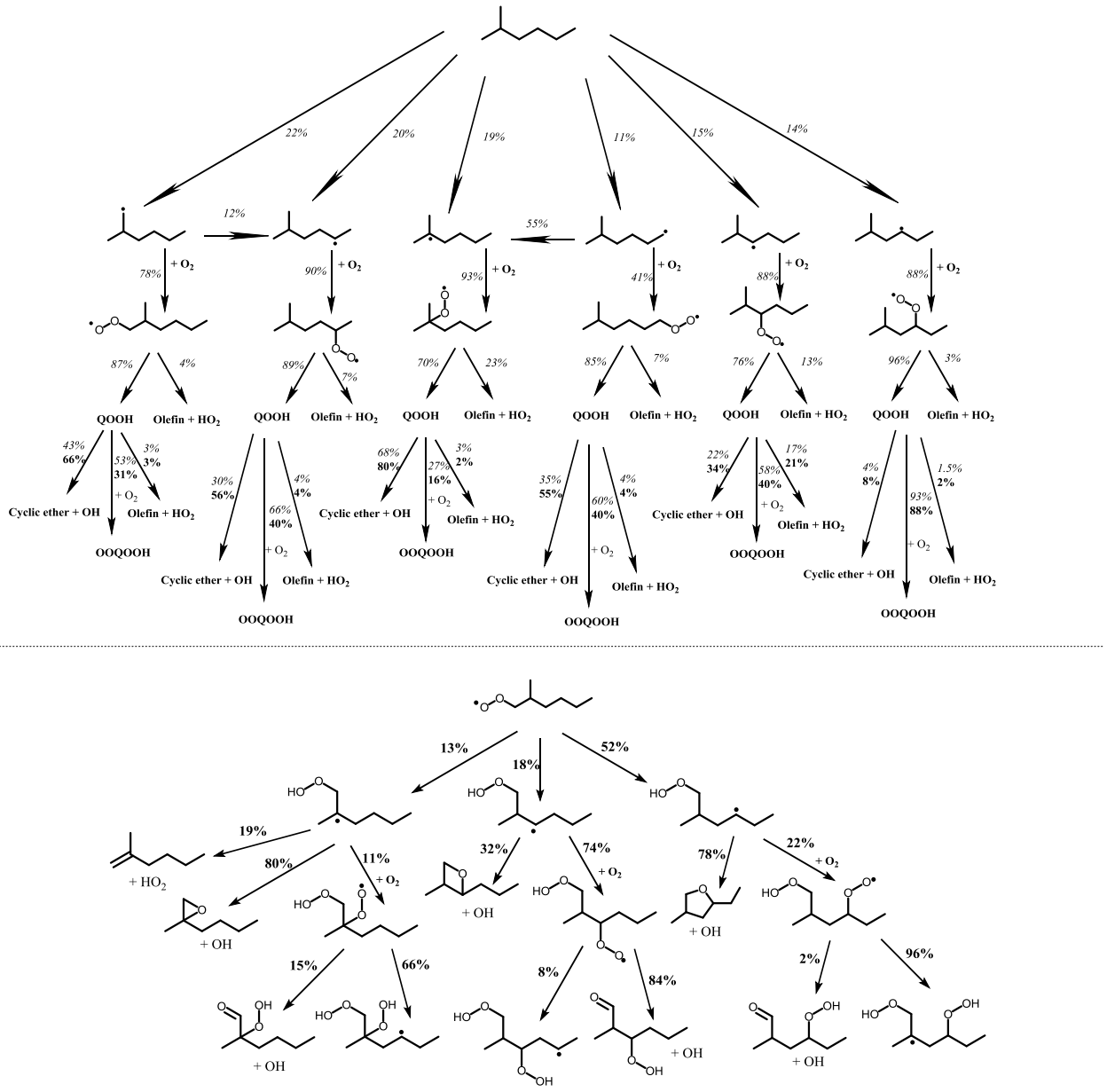

Figure 16: Flux analysis at 20 bar, 800K and 20% consumption of 2-methylhexane, *italic%* updated mechanism, **Bold%** tuned mechanism

4.2 Automatic model optimization

In addition to manual tuning, an automatic mechanism optimization technique based on reaction rate rules[21] was used to improve the model's predictive ability and minimize differences between model and experiments. This technique was developed based on the work of

Frenklach[46]. Uncertainty minimization using polynomial chaos expansion MUM-PCE by Sheen and Wang[47] was used to calibrate the rate rules. Sensitivity analysis was first performed at the conditions of interest to select the important rate rules. The pre-exponential factors of the rate rules were then systematically calibrated within their specified uncertainty bounds through the minimization of the deviations between model responses and measurements.

46 rate rules are selected for calibration due to their high sensitivity and are listed in Table 5 along with their related pre-exponential factors and uncertainty limits. For the H-atom abstraction from fuel by OH radicals, uncertainties are defined as 1.5, as these rate rules are accurately measured by Sivaramakrishnan et al.[40] and Badra et al.[41]. Note that, for the automatic calibration, the rate rules proposed by Bugler et al.[5] for low temperature classes 11, 15, 16, 23, and 25 (Table 5) are incorporated in the prior set, as detailed information about rate uncertainties are provided. A factor of 4 was used for the remaining rate rules, as no values were available in the literature. Note that the rate rules are treated as uniformly distributed in their error bounds, as suggested by Bugler et al.[5].

Optimized rate rules were mainly the H-abstraction from fuel by various radicals and rate controlling reaction classes in the low temperature reaction mechanism. For example, classes 11, 15, 26, and 27 are essential steps in the low temperature chain branching sequence. In contrast, the acceleration of the concerted elimination of RO_2 and the cyclic ethers formation can retard ignition at low temperatures.

Calibrating all these sensitive rate rules generated an optimized mechanism. The modified set of rate rules is shown in Table 5, which is specifically optimized for 2-methylhexane. It can be seen that a few rate rules were modified strongly. The reason is that uniform distributions were

specified to the original parameters, which gives constant probability to the parameter values within uncertainty bounds.

The ignition delay profiles calculated using the optimized model are presented in Figure 17. It is seen that the optimized model agrees very well with the measurements. A notable improvement is observed in first stage ignition delay time simulations at both lean and stoichiometric conditions. The optimization framework successfully modified the rate rules within their uncertainty bounds and minimized the disagreement between model and experiment.

Table 5: Unoptimized (Ao) and optimized (A) pre-exponential factors per H-atom basis

Class	Rate rule	Uncertainty	Ao[a]	A
C1	Fuel decomposition→CH_3 and alkyl radical	[4.0, 4.0]	1.00E+13	4.00E+12
C1	Fuel decomposition→ alkyl radicals	[4.0, 4.0]	8.00E+12	3.20E+13
C2	H-atom abstraction from the fuel by H (primary carbon site)	[4.0, 4.0]	2.22E+05	1.75E+05
C2	H-atom abstraction from the fuel by H (secondary carbon site)	[4.0, 4.0]	6.50E+05	1.72E+05
C2	H-atom abstraction from the fuel by H (tertiary carbon site)	[4.0, 4.0]	6.02E+05	1.18E+06
C2	H-atom abstraction from the fuel by OH (P1)	[1.5, 1.5]	4.55E+06	6.82E+06
C2	H-atom abstraction from the fuel by OH (S01)	[1.5, 1.5]	3.53E+09	2.35E+09
C2	H-atom abstraction from the fuel by OH (S11)	[1.5, 1.5]	2.86E+06	1.90E+05
C2	H-atom abstraction from the fuel by OH (P2)	[1.5, 1.5]	5.58E+05	3.72E+05
C2	H-atom abstraction from the fuel by OH (T001)	[1.5, 1.5]	3.43E+08	2.28E+08
C2	H-atom abstraction from the fuel by OH (S21)	[1.5, 1.5]	6.45E+08	7.08E+08
C2	H-atom abstraction from the fuel by HO_2 (primary carbon site)	[4.0, 4.0]	6.80E+00	5.08E+00
C2	H-atom abstraction from the fuel by HO_2 (secondary carbon site)	[4.0, 4.0]	3.16E+01	7.90E+00

C2	H-atom abstraction from the fuel by HO_2 (tertiary carbon site)	[4.0, 4.0]	6.50E+02	2.60E+03
C2	H-atom abstraction from the fuel by CH_3 (secondary carbon site)	[4.0, 4.0]	7.55E-01	2.68E-01
C2	H-atom abstraction from the fuel by O_2 (secondary carbon sites)	[4.0, 4.0]	1.00E+13	1.58E+13
C2	H-atom abstraction from the fuel by CH_3O_2 (secondary carbon site)	[4.0, 4.0]	5.10E+00	1.49E+00
C2	H-atom abstraction from the fuel by CH_3O_2 (tertiary carbon site)	[4.0, 4.0]	2.06E+02	5.40E+01
C3	Alkyl radical (R) decomposition→ alkene and H (secondary carbon site)	[4.0, 4.0]	2.50E+11	1.00E+12
C4	Alkyl radical (R) isomerization (6m, P → S)	[4.0, 4.0]	1.82E+02	2.05E+02
C4	Alkyl radical (R) isomerization (6m, T → P)	[4.0, 4.0]	4.86E+01	9.72E+01
C5	H-atom abstraction from alkene by OH	[4.0, 4.0]	3.28E+08	1.23E+08
C9	Alkene decomposition	[4.0, 4.0]	2.50E+16	6.07E+16
C11	Addition of O_2 to alkyl radicals (R) (primary carbon site)	[2.2, 1.7]	1.30E+11	2.21E+11
C11	Addition of O_2 to alkyl radicals (R) (secondary carbon site)	[1.7, 2.1]	1.51E+15	3.17E+15
C15	Alkyl peroxy radical isomerization (1,4s)	[3.1, 4.2]	2.33E+07	9.80E+07
C15	Alkyl peroxy radical isomerization (1,5s)	[2.3, 2.2]	8.20E+10	3.57E+10
C15	Alkyl peroxy radical isomerization (1,6s)	[2.3, 1.6]	7.05E+08	3.07E+08
C15	Alkyl peroxy radical isomerization (1,4t)	[2.0, 1.9]	5.63E+10	5.39E+10
C15	Alkyl peroxy radical isomerization (1,6t)	[1.6, 1.5]	1.29E+07	8.04E+06
C15	Alkyl peroxy radical isomerization (1,5t)	[2.0, 2.1]	1.82E+07	3.82E+07
C15	Alkyl peroxy radical isomerization (1,7t)	[1.3, 1.2]	2.96E+09	3.55E+09
C16	Concerted eliminations (RO_2→ alkene + HO_2)	[2.2, 2.8]	2.89E+09	8.08E+09
C23	QOOH→ cyclic ether (4m) + OH	[11.1, 35.8]	4.58E+15	5.53E+16
C23	QOOH→ cyclic ether (5m) + OH	[6.2, 7.4]	3.50E+10	5.65E+09

C25	QOOH→ β-scission products	[6.0, 8.5]	5.82E+05	7.15E+05
C26	Addition of O_2 to QOOH (primary carbon site)	[4.0, 4.0]	6.51E+10	2.60E+11
C26	Addition of O_2 to QOOH (secondary carbon site)	[4.0, 4.0]	7.54E+14	2.70E+15
C26	Addition of O_2 to QOOH (tertiary carbon site)	[4.0, 4.0]	1.23E+11	4.92E+11
C27	Isomerization of OOQOOH (6m, OOH-P, OO-S)	[4.0, 4.0]	5.49E+03	1.38E+03
C27	Isomerization of OOQOOH (6m, OOH-S, OO-S)	[4.0, 4.0]	1.75E+02	4.38E+02
C27	Isomerization of OOQOOH (6m, OOH-S, OO-T)	[4.0, 4.0]	8.20E+10	1.59E+11
C28	Decomposition of ketohydroperoxide	[4.0, 4.0]	1.00E+16	2.50E+15
C29	Cyclic ether reactions with OH	[4.0, 4.0]	2.50E+12	2.21E+12
C31	Alternative isomerization of OOQOOH→ $P(OOH)_2$ (6m, S)	[4.0, 4.0]	1.64E+11	4.10E+10
C33	$P(OOH)_2$→ cyclic ether (3m) + OH	[4.0, 4.0]	2.28E+08	9.13E+08

[a] upper and lower uncertainty bounds and their definitions are obtained from Bugler et al.[5] when available and an uncertainty of 4 is used for the remaining rate rules.

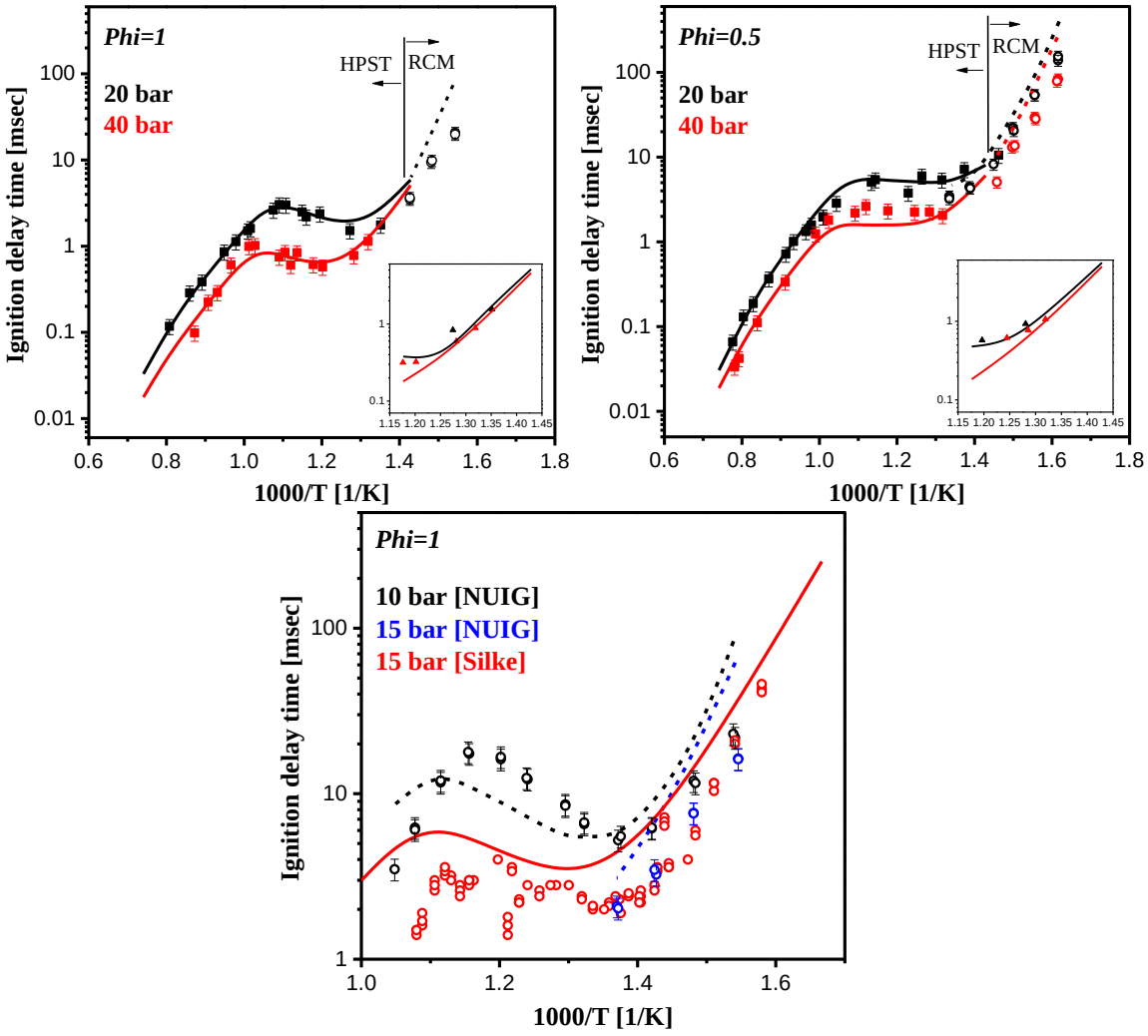

Figure 17. Final model after optimization compared to HPST (solid line and square symbols) and RCM (dashed line and circle symbols) data. The insets illustrate 1st stage ignition measured in the HPST.

4.3 Analysis of reactivity at low temperatures

The aforementioned modifications to the kinetic model successfully improved agreement with experimental data under shock tube conditions. However, the agreement with ignition delay times measured in the RCM at relatively lower temperatures (e.g., below 715 K) did not improve when the model was optimized. Both the manual and automated optimization schemes only modified pre-exponential rate coefficients, which applies a uniform change in the rate constant at

all temperatures. Figure 18 demonstrates that RCM ignition delay times at low temperatures are primarily sensitive to the activation energy for the decomposition of ketohydroperoxides, hydroperoxy cyclic ethers, and olefinic-hydroperoxides. As mentioned previously, the activation energy (Ea) used in the model is 42.3 kcal/mol, which is close to the 43 kcal/mol value calculated by Jalan et al.[45]. We found that modifying the activation energy to 41.6 kcal/mol provided better agreement with the experimental data.

While modifying the activation energy appears to resolve the discrepancy between model and experiment, the revised value is further from the theoretical calculations by Jalan et al.[45]. Recently Wang and coworkers[48-50] discovered a previously unconsidered 3rd O_2 addition reaction scheme in the low temperature oxidation of alkanes. Wang and Sarathy[49] showed that including these additional chain branching reactions accelerates simulated ignition delay times for *n*-alkanes at low temperatures and high pressures. In a recent work on jet stirred reactor oxidation of 2-methylhexane, we [50] added the 3rd O_2 addition pathways to the present paper's manually tuned kinetic model. Wang et al.[50] discuss the kinetic modeling of 3rd O_2 addition pathways in detail. Figure 18 shows that including the 3rd O_2 addition pathways improves agreement with the RCM experimental data without the need to modify the activation energy for decomposition of ketohydroperoxides, hydroperoxy cyclic ethers, and olefinic-hydroperoxides. Thus, these additional reaction pathways improve the predictive capabilities of the model without the need for additional tuning/re-tuning of rate constants.

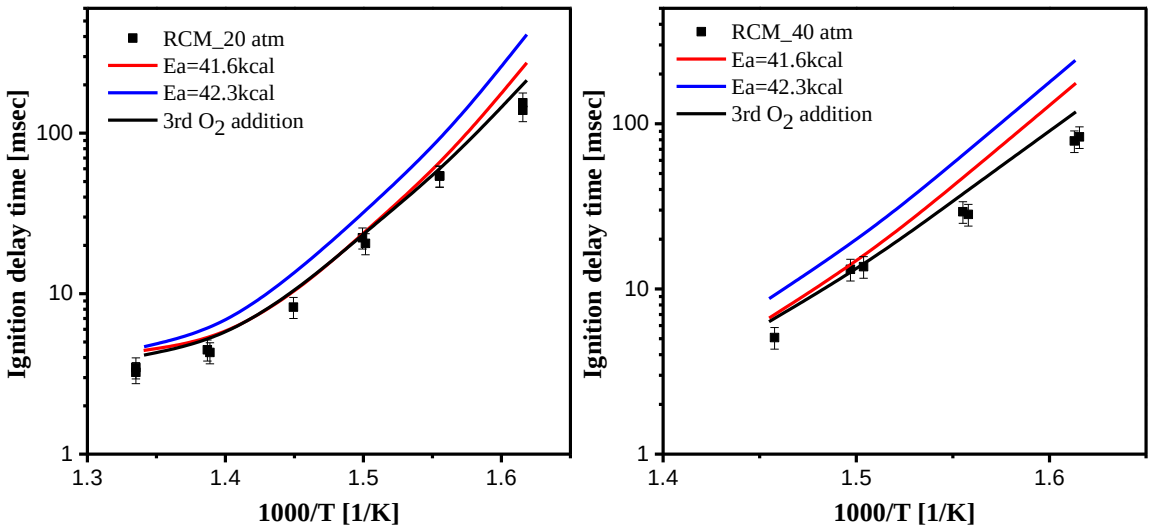

Figure 18: Simulated ignition delay time compared to RCM data at 20 and 40 bar, φ =0.5

5 Conclusion

In this work, thermodynamic data and the kinetic mechanism of 2-methylhexane have been updated using updated group values and accurately measured and calculated rate rules, respectively. Thermodynamic updates, especially of low temperature species, shift the equilibria of low temperature reactions towards inhibition of reactivity. The updated rate rules also cause a significant effect on model behavior, particularly at low temperatures.

Alternative pathways have also been added to the mechanism, which result in increased reactivity and faster ignition due to the importance of hydroperoxy cyclic ether + OH formation from $P(OOH)_2$ radicals. However, the exact effect of these added pathways is not yet well addressed due to the analogies used to assign their rate coefficients. In order to evaluate the importance of these pathways and their contribution to fuel reactivity, it is essential to measure or calculate their rate coefficients precisely.

The updated model has been compared against new ignition delay data measured in a high pressure shock tube and a rapid compression machine at pressures of 10, 15, 20 and 40 bar, at lean and stoichiometric conditions. The results show that upon incorporating the thermodynamic

and kinetic updates, the updated model is more reactive at low and intermediate temperatures. In order to minimize discrepancies between the model and experiments, two approaches were adopted: manual tuning and automated optimization techniques. Both methods led to improvements in model predictions against HPST and RCM experimental data, by appropriately constraining branching ratios between various low temperature radical chain branching, propagation, and termination pathways. Finally, additional chain branching pathways in the form of the 3rd O_2 addition reaction scheme are shown to improve predictions at low temperatures; the kinetics of these reactions should be the focus of future experimental and theoretical research.

6 Supporting Information

Tabulation of the HPST and RCM experimental data, comparison between original and updated rate rules, low temperature pathways of c7h15-2b and c7h15-2d, simulated ignition delay time using updated and original models compared to experimental data and species dictionary. Tuned and optimized 2-methyl-hexane chemical kinetic models. This material is available free of charge via the Internet at http://pubs.acs.org

7 Author information

Corresponding Author

S. Mani Sarathy, E-mail: mani.sarathy@kaust.edu.sa Phone no: +966 54 4700142

8 Acknowledgment

The research reported in this publication was supported by Saudi Aramco under the FUELCOM program and by the King Abdullah University of Science and Technology (KAUST) with competitive research funding given to the Clean Combustion Research Center (CCRC). The

work at RWTH Aachen University was performed within the Cluster of Excellence "Tailor-Made Fuels from Biomass", which is funded by the Excellence Initiative of the German federal state governments to promote science and research at German universities. The research at NUIG leading to these results has received funding from the People Programme (Marie Curie Actions) of the European Union's Seventh Framework Programme FP7/2007-2013/ under REA grant agreement n° 607214.

9 References

1. Susnow, R. G.; Dean, A. M.; Green, W. H.; Peczak, P.; Broadbelt, L. J., Rate-Based Construction of Kinetic Models for Complex Systems. *J Phys Chem A* **1997,** *101* (20), 3731-3740 10.1021/jp9637690.
2. Benson, S. W., The Kinetics and Thermochemistry of Chemical Oxidation with Application to Combustion and Flames. *Prog Energ Combust* **1981,** *7* (2), 125-134 http://dx.doi.org/10.1016/0360-1285(81)90007-1.
3. Benson, S. W., *Thermochemical Kinetics*. 2nd ed.; Wiley-VCH Verlag GmbH & Co. KGaA: 1976.
4. Benson, S. W.; Norman, C., Current Status of Group Additivity. In *Computational Thermochemistry*, American Chemical Society: 1998; Vol. 677, pp 20-46.
5. Bugler, J.; Somers, K. P.; Silke, E. J.; Curran, H. J., Revisiting the Kinetics and Thermodynamics of the Low-Temperature Oxidation Pathways of Alkanes: A Case Study of the Three Pentane Isomers. *J Phys Chem A* **2015,** *119* (28), 7510-7527 10.1021/acs.jpca.5b00837.
6. Zhang, K.; Banyon, C.; Togbé, C.; Dagaut, P.; Bugler, J.; Curran, H. J., An Experimental and Kinetic Modeling Study of N-Hexane Oxidation. *Combust Flame* **2015,** *162* (11), 4194-4207 http://dx.doi.org/10.1016/j.combustflame.2015.08.001.
7. Silke, E. J.; Curran, H. J.; Simmie, J. M.; Pitz, W. J.; Westbrook, C. K., A Rapid Compression Machine Modelling Study of the Heptane Isomers. In *European Combustion Meeting*, Louvain-la-Neuve, Belgium, 2005.
8. Curran, H. J.; Gaffuri, P.; Pitz, W. J.; Westbrook, C. K., A Comprehensive Modeling Study of N-Heptane Oxidation. *Combust Flame* **1998,** *114* (1–2), 149-177 http://dx.doi.org/10.1016/S0010-2180(97)00282-4.
9. Healy, D.; Kalitan, D. M.; Aul, C. J.; Petersen, E. L.; Bourque, G.; Curran, H. J., Oxidation of C1−C5 Alkane Quinternary Natural Gas Mixtures at High Pressures. *Energ Fuel* **2010,** *24* (3), 1521-1528 10.1021/ef9011005.
10. Sharma, S.; Raman, S.; Green, W. H., Intramolecular Hydrogen Migration in Alkylperoxy and Hydroperoxyalkylperoxy Radicals: Accurate Treatment of Hindered Rotors. *J Phys Chem A* **2010,** *114* (18), 5689-5701 10.1021/jp9098792.
11. Villano, S. M.; Huynh, L. K.; Carstensen, H. H.; Dean, A. M., High-Pressure Rate Rules for Alkyl + O_2 Reactions. 1. The Dissociation, Concerted Elimination, and Isomerization Channels of the Alkyl Peroxy Radical. *J Phys Chem A* **2011,** *115* (46), 13425-42 10.1021/jp2079204.

12. Miyoshi, A., Systematic Computational Study on the Unimolecular Reactions of Alkylperoxy (RO_2), Hydroperoxyalkyl (Qooh), and Hydroperoxyalkylperoxy (O_2QOOH) Radicals. *J Phys Chem A* **2011,** *115* (15), 3301-25 10.1021/jp112152n.
13. Villano, S. M.; Huynh, L. K.; Carstensen, H. H.; Dean, A. M., High-Pressure Rate Rules for Alkyl + O_2 Reactions. 2. The Isomerization, Cyclic Ether Formation, and Beta-Scission Reactions of Hydroperoxy Alkyl Radicals. *J Phys Chem A* **2012,** *116* (21), 5068-89 10.1021/jp3023887.
14. Villano, S. M.; Carstensen, H. H.; Dean, A. M., Rate Rules, Branching Ratios, and Pressure Dependence of the HO_2 + Olefin Addition Channels. *J Phys Chem A* **2013,** *117* (30), 6458-73 10.1021/jp405262r.
15. Burke, S. M.; Simmie, J. M.; Curran, H. J., Critical Evaluation of Thermochemical Properties of C1–C4 Species: Updated Group-Contributions to Estimate Thermochemical Properties. *J. Phys. Chem. Ref. Data* **2015,** *44* (1), 013101 doi:http://dx.doi.org/10.1063/1.4902535.
16. Sarathy, S. M.; Kukkadapu, G.; Mehl, M.; Wang, W.; Javed, T.; Park, S.; Oehlschlaeger, M. A.; Farooq, A.; Pitz, W. J.; Sung, C.-J., Ignition of Alkane-Rich FACE Gasoline Fuels and Their Surrogate Mixtures. *Proc Combust Inst* **2015,** *35* (1), 249-257 http://dx.doi.org/10.1016/j.proci.2014.05.122.
17. Westbrook, C. K.; Pitz, W. J.; Curran, H. C.; Boercker, J.; Kunrath, E., Chemical Kinetic Modeling Study of Shock Tube Ignition of Heptane Isomers. *Int J Chem Kinet* **2001,** *33* (12), 868-877 10.1002/kin.10020.
18. Sarathy, S. M.; Westbrook, C. K.; Mehl, M.; Pitz, W. J.; Togbe, C.; Dagaut, P.; Wang, H.; Oehlschlaeger, M. A.; Niemann, U.; Seshadri, K.; Veloo, P. S.; Ji, C.; Egolfopoulos, F. N.; Lu, T., Comprehensive Chemical Kinetic Modeling of the Oxidation of 2-Methylalkanes from C7 to C20. *Combust Flame* **2011,** *158* (12), 2338-2357 10.1016/j.combustflame.2011.05.007.
19. Curran, H. J.; Gaffuri, P.; Pitz, W. J.; Westbrook, C. K., A Comprehensive Modeling Study of Iso-Octane Oxidation. *Combust Flame* **2002,** *129* (3), 253-280 http://dx.doi.org/10.1016/S0010-2180(01)00373-X.
20. Silke, E. J.; Curran, H. J.; Simmie, J. M., The Influence of Fuel Structure on Combustion as Demonstrated by the Isomers of Heptane: A Rapid Compression Machine Study. *Proc Combust Inst* **2005,** *30* (2), 2639-2647 http://dx.doi.org/10.1016/j.proci.2004.08.180.
21. Cai, L.; Pitsch, H., Mechanism Optimization Based on Reaction Rate Rules. *Combust Flame* **2014,** *161* (2), 405-415 http://dx.doi.org/10.1016/j.combustflame.2013.08.024.
22. Cai, L.; Pitsch, H.; Sarathy, S. M.; Mohamed, Y., Samah; Raman, V.; Bugler, J.; Curran, H. J., Optimized Reaction Mechanism Rate Rules for Normal Alkanes. *Combust Flame* **2015**,
23. Nguyen, T. T. N.; Wilgeroth, J. M.; Proud, W. G., Controlling Blast Wave Generation in a Shock Tube for Biological Applications. *J Phys Conf Ser.* **2014,** *500* (14), 142025
24. Park, S.; Mannaa, O.; Khaled, F.; Bougacha, R.; Mansour, M. S.; Farooq, A.; Chung, S. H.; Sarathy, S. M., A Comprehensive Experimental and Modeling Study of 2-Methylbutanol Combustion. *Combust Flame* **2015,** *162* (5), 2166-2176 http://dx.doi.org/10.1016/j.combustflame.2015.01.014.
25. Affleck, W. S.; Thomas, A., An Opposed Piston Rapid Compression Machine for Preflame Reaction Studies. *P I Mech Eng* **1969,** *183* (1), 365-385
26. Brett, L.; Macnamara, J.; Musch, P.; Simmie, J. M., Simulation of Methane Autoignition in a Rapid Compression Machine with Creviced Pistons. *Combust Flame* **2001,** *124* (1–2), 326-329 http://dx.doi.org/10.1016/S0010-2180(00)00193-0.

27. Würmel, J.; Simmie, J. M., CFD Studies of a Twin-Piston Rapid Compression Machine. *Combust Flame* **2005,** *141* (4), 417-430 http://dx.doi.org/10.1016/j.combustflame.2005.01.015.
28. Würmel, J.; Silke, E. J.; Curran, H. J.; Ó Conaire, M. S.; Simmie, J. M., The Effect of Diluent Gases on Ignition Delay Times in the Shock Tube and in the Rapid Compression Machine. *Combust Flame* **2007,** *151* (1–2), 289-302 http://dx.doi.org/10.1016/j.combustflame.2007.06.010.
29. Fish, A.; Haskell, W. W.; Read, I. A., The Non-Isothermal Oxidation of 2-Methylpentane. Iii. The Reaction at High Pressure. *Proc R Soc Lon Ser-A* **1969,** *313* (1513), 261-297
30. Mittal, G.; Sung, C.-J., Aerodynamics inside a Rapid Compression Machine. *Combust Flame* **2006,** *145* (1–2), 160-180 http://dx.doi.org/10.1016/j.combustflame.2005.10.019.
31. Das, A. K.; Uddi, M.; Sung, C.-J., Two-Line Thermometry and H2o Measurement for Reactive Mixtures in Rapid Compression Machine near 7.6 Mm. *Combust Flame* **2012,** *159* (12), 3493-3501 http://dx.doi.org/10.1016/j.combustflame.2012.06.020.
32. Burke, S. M.; Metcalfe, W.; Herbinet, O.; Battin-Leclerc, F.; Haas, F. M.; Santner, J.; Dryer, F. L.; Curran, H. J., An Experimental and Modeling Study of Propene Oxidation. Part 1: Speciation Measurements in Jet-Stirred and Flow Reactors. *Combust Flame* **2014,** *161* (11), 2765-2784 http://dx.doi.org/10.1016/j.combustflame.2014.05.010.
33. *Chemkin-Pro 15112*, San Diego, 2012.
34. Ritter, E. R., Therm: A Computer Code for Estimating Thermodynamic Properties for Species Important to Combustion and Reaction Modeling. *J Chem Inf Comp Sci* **1991,** *31* (3), 400-408 10.1021/ci00003a006.
35. Benson, S. W.; Buss, J. H., Additivity Rules for the Estimation of Molecular Properties. Thermodynamic Properties. *The Journal of Chemical Physics* **1958,** *29* (3), 546 10.1063/1.1744539.
36. Sabbe, M. K.; Saeys, M.; Reyniers, M.-F.; Marin, G. B.; Van Speybroeck, V.; Waroquier, M., Group Additive Values for the Gas Phase Standard Enthalpy of Formation of Hydrocarbons and Hydrocarbon Radicals. *J Phys Chem A* **2005,** *109* (33), 7466-7480 10.1021/jp050484r.
37. Sabbe, M. K.; De Vleeschouwer, F.; Reyniers, M.-F.; Waroquier, M.; Marin, G. B., First Principles Based Group Additive Values for the Gas Phase Standard Entropy and Heat Capacity of Hydrocarbons and Hydrocarbon Radicals. *J Phys Chem A* **2008,** *112* (47), 12235-12251 10.1021/jp807526n.
38. Cohen, N.; Benson, S. W., In *The Chemistry of Alkanes and Cycloalkanes*, Patai, S.; Rappoport, Z., Eds. John Wiley & Sons, Ltd: 1992; pp 215-287.
39. Goldsmith, C. F.; Green, W. H.; Klippenstein, S. J., Role of O_2 + QOOH in Low-Temperature Ignition of Propane. 1. Temperature and Pressure Dependent Rate Coefficients. *J Phys Chem A* **2012,** *116* (13), 3325-46 10.1021/jp210722w.
40. Sivaramakrishnan, R.; Michael, J. V., Rate Constants for OH with Selected Large Alkanes: Shock-Tube Measurements and an Improved Group Scheme. *J Phys Chem A* **2009,** *113* (17), 5047-5060 10.1021/jp810987u.
41. Badra, J.; Elwardany, A.; Farooq, A., Shock Tube Measurements of the Rate Constants for Seven Large Alkanes + OH. *Proc Combust Inst* **2015,** *35* (1), 189-196 http://dx.doi.org/10.1016/j.proci.2014.05.098.
42. Cohen, N., Are Reaction Rate Coefficients Additive? Revised Transition State Theory Calculations for OH + Alkane Reactions. *Int J Chem Kinet* **1991,** *23* (5), 397-417 10.1002/kin.550230506.

43. Orme, J. P.; Curran, H. J.; Simmie, J. M., Experimental and Modeling Study of Methyl Cyclohexane Pyrolysis and Oxidation. *J Phys Chem A* **2005,** *110* (1), 114-131 10.1021/jp0543678.
44. Merchant, S. S.; Goldsmith, C. F.; Vandeputte, A. G.; Burke, M. P.; Klippenstein, S. J.; Green, W. H., Understanding Low-Temperature First-Stage Ignition Delay: Propane. *Combust Flame* **2015,** *162* (10), 3658-3673 http://dx.doi.org/10.1016/j.combustflame.2015.07.005.
45. Jalan, A.; Alecu, I. M.; Meana-Pañeda, R.; Aguilera-Iparraguirre, J.; Yang, K. R.; Merchant, S. S.; Truhlar, D. G.; Green, W. H., New Pathways for Formation of Acids and Carbonyl Products in Low-Temperature Oxidation: The Korcek Decomposition of γ-Ketohydroperoxides. *J Am Chem Soc* **2013,** *135* (30), 11100-11114 10.1021/ja4034439.
46. Frenklach, M., Systematic Optimization of a Detailed Kinetic Model Using a Methane Ignition Example. *Combust Flame* **1984,** *58* (1), 69-72 http://dx.doi.org/10.1016/0010-2180(84)90079-8.
47. Sheen, D. A.; Wang, H., The Method of Uncertainty Quantification and Minimization Using Polynomial Chaos Expansions. *Combust Flame* **2011,** *158* (12), 2358-2374 http://dx.doi.org/10.1016/j.combustflame.2011.05.010.
48. Wang, Z.; Zhang, L.; Moshammer, K.; Popolan-Vaida, D. M.; Shankar, V. S. B.; Lucassen, A.; Hemken, C.; Taatjes, C. A.; Leone, S. R.; Kohse-Höinghaus, K.; Hansen, N.; Dagaut, P.; Sarathy, S. M., Additional Chain-Branching Pathways in the Low-Temperature Oxidation of Branched Alkanes. *Combust Flame*, http://dx.doi.org/10.1016/j.combustflame.2015.11.035.
49. Wang, Z.; Sarathy, S. M., Third O_2 Addition Reactions Promote the Low-Temperature Auto-Ignition of N-Alkanes. *Combust Flame*, http://dx.doi.org/10.1016/j.combustflame.2015.12.020.
50. Wang, Z.; Mohamed, S. Y.; Zhang, L.; Moshammer, K.; Popolan-Vaida, D. M.; Shankar, V. S. B.; Lucassen, A.; Ruwe, L.; Hansen, N.; Dagaut, P.; Sarathy, S. M., New insights into the low-temperature oxidation of 2-methylhexan. *Submitted to Proc. Combust. Inst.* **2015**,

Table of Contents Graphic: